Chapter 1

PHOTONEUTRON CROSS SECTIONS ON NATURALLY PRESENT OSMIUM ISOTOPES

S. S. Belyshev, B. S. Ishkhanov*, V. V. Khankin A. A. Kuznetsov, V. N. Orlin, N. N. Peskov, M. E. Stepanov, K. A. Stopani, V. V. Varlamov
Lomonosov Moscow State University, Department of Physics,
Moscow, 119991 Russia
Lomonosov Moscow State University, Skobeltsyn Institute of Nuclear Physics,
Moscow, 119991 Russia

PACS 25.20.-x, 24.60.Dr **Keywords:** photonuclear reactions, activation technique, nuclear models

Contents

1. Introduction **2**

2. The liquid drop model **3**

3. Nuclear shell model **5**

*E-mail address: bsi@depni.sinp.msu.ru

4. Interaction of photons with atomic nuclei **7**

5. Low-lying excited states of the Os isotopes **9**

6. Giant dipole resonance **12**
6.1. GDR splitting in axially symmetric nuclei 13
6.2. Triaxial nuclei 14
6.3. Effects of isospin 15

7. Combined model of photonuclear reactions **16**
7.1. Photoabsorption cross section 17
7.2. Emission of particles 18
7.2.1. Isospin effects 18
7.2.2. Effect of the structure of the GDR on semi-direct reactions 20

8. Evaluated cross sections of photoneutron reactions **21**

9. Photon activation technique **33**

10. Synthesis of stable isotopes in nature **35**

11. Conclusions **39**

1. Introduction

The nucleus is a bound system of protons and neutrons. Different types of nucleon interactions are manifestly exposed in the properties of nuclei. The nucleus is a complex system which is affected by different aspects of the strong, electromagnetic, and weak interactions, and, therefore, different models are used for their description.

Independent motion of nucleons in the atomic nucleus is one of the main properties of nuclear matter. In this sense the nucleus is similar to a degenerate Fermi gas, i.e., a rather dense ideal gas, composed of fermions, or particles that obey the Pauli exclusion principle. However, the analogy is fairly limited, because the nucleus has a finite size and an almost constant density, and it does not tend to occupy the whole available volume, which is characteristic of a gas. The nucleons maintain a constant density and are held together in the nucleus not unlike a liquid droplet, which is called the Fermi liquid by analogy with the Fermi gas model. Despite a certain similaraty of non-shperical, or deformed nuclei with solids further analogies of this kind are very approximate due to the prevalent role of single particle motions. A combination of complex short-range nuclear forces and long-range Couloumb interactions makes nuclear matter a unique state with properties that are not observed in the "macroscopic" world.

There are 41 known isotopes of osmium, which gives important information about the dependence of the nuclear properties on N. The present review has the following structure. The first and the second sections describe two nuclear models: the liquid drop model and the nuclear shell model, that is, the examplary macroscopic and microscopic approaches to description of the nuclei. Section 3 briefly describes the effects that play the most important

role during the interaction of photons with a nucleus. The low-lying excited states of the stable isotopes of Os are described in section 5, and section 6 gives a brief description of the most important effect of interaction of photons with nuclei, the so-called giant dipole resonance, which enhances the photon absorption cross section in the energy range 7–40 MeV. A combined model of photonuclear reactions which is used to calculate cross sections of multiparticle photonuclear reactions is described in section 7. Based on this model and experimental results from other measurements in section 8 a set of evaluated cross sections of partial photoneutron reactions on Os is obtained. In section 9 the photon activation technique is used to measure experimental yields of multinucleon photonuclear reactions. In the last section astrophysical aspects of synthesis of the isotopes of Os are discussed.

2. The liquid drop model

Mass is one of the main properties of nuclei. Knowing the nuclear masses one can calculate different characteristics of nuclear decays. The atomic nucleus is a system of N neutrons n and Z protons p bound by nuclear forces. To split a nucleus with a mass $M(A,Z)$ (where $A = N + Z$ is the mass number) into separate nucleons, an energy should be introduced to the system. This energy, called the nuclear binding energy E_{bind}, is determined by the difference of the masses of the nucleus and unbound nucleons:

$$M(A,Z)c^2 + E_{\text{bind}} = [Zm_p + (A-Z)m_n]c^2. \tag{1}$$

The liquid drop model is usually associated with the semiempirical mass formula written in 1935 by C. Weizsäcker [1] using the analogy between a nucleus and a charged liquid drop with radius $R = r_0 A^{1/3}$:

$$E_{\text{bind}}(A,Z) = \alpha_1 A - \alpha_2 A^{2/3} - \alpha_3 \frac{Z^2}{A^{1/3}} - \alpha_4 \frac{1}{4}\left(\frac{A}{2} - Z\right)^2 + \alpha_5 A^{-3/4}. \tag{2}$$

The first term in the binding energy $E_{\text{vol}} = \alpha_1 A$ is proportional to the mass number A and represents the volume energy of the nucleus. The second term is the surface energy $E_{\text{surf}} = \alpha_2 A^{2/3}$ that accounts for the surface tension effects. Unlike the molecules of classical liquids nucleons on the nuclear surface have an excess of both potential and kinetic energies. The third term $E_{\text{Coul}} = \alpha_3 \frac{Z^2}{A^{1/3}}$ corresponds to the Coulomb repulsion of protons, assuming that the electrical charge of protons is distributed uniformly over the nucleus with radius $R = r_0 A^{1/3}$. Other terms have no direct classical analogy. The fourth term is the nuclear symmetry energy $E_{\text{sym}} = \alpha_4 \frac{1}{4}\left(\frac{A}{2} - Z\right)^2$, which reflects the tendency of having approximately equal numbers of protons and neutrons, and the nuclear odd-even, or pairing, effect is taken into account via the pairing energy $E_{\text{p}} = \alpha_5 A^{-3/4}$. A set of the values of the coefficients α_1–α_5 that appropriately describe the experimental binding energies in the whole range of nuclear masses is the following:

$$\alpha_1 = 15.75 \text{ MeV}, \quad \alpha_2 = 17.8 \text{ MeV}, \quad \alpha_3 = 0.71 \text{ MeV}, \quad \alpha_4 = 94.8 \text{ MeV}, \tag{3}$$

$$\alpha_5 = \begin{cases} +34 \text{ MeV} & \text{for even-even nuclei} \\ 0 & \text{for odd nuclei} \\ -34 \text{ MeV} & \text{for odd-odd nuclei.} \end{cases}$$

The liquid drop model describes the nuclear binding energies with a relative accuracy of up to about 1%.

Table 1. Main characteristics of known isotopes of osmium: mass number A, number of neutrons N, ground state spin and parity J^P, binding energy per nucleon ε, proton and neutron separation energies B_p and B_n, half life $T_{1/2}$ or isotopic abundance (e.t.a.), percentages of α- and β-decay channels

A	N	J^P	ε	B_n	B_p	$T_{1/2}$ or e.t.a.	$\%\alpha$	$\%\beta^-$	$\%\beta^+$
161	85	$7/2^-$	7765		577	640 μs	100	0	0
162	86	0^+	7794	12355	901	2.1 ms	100	0	0
163	87	$7/2^-$	7807	9954	1173	5.5 ms	100	0	0
164	88	0^+	7833.599	12159	1754.17	21 ms	98	0	2
165	89	$7/2^-$	7843	9394	1561	71 ms	60	0	40
166	90	0^+	7866.368	11713	2082.09	216 ms	72	0	28
167	91	$7/2^-$	7873.975	9136.67	1897.53	839 ms	51	0	49
168	92	0^+	7895.892	11556.05	2433	2.1 s	43	0	57
169	93	$5/2^-$	7901.285	8807.36	2217.02	3.46 s	13.7	0	86.3
170	94	0^+	7921.130	11274.84	2806.26	7.37 s	9.5	0	90.5
171	95	$5/2^-$	7924.211	8448.09	2674.44	8.3 s	1.8	0	98.2
172	96	0^+	7942.162	11011.72	3282.32	19.2 s	1.1	0	98.9
173	97	$5/2^-$	7944.033	8265.86	3200.83	22.4 s	0.4	0	99.6
174	98	0^+	7959.459	10628.23	3730.19	44 s	0.024	0	99.976
175	99	$5/2^-$	7960.728	8181.41	3721.06	1.4 m	0	0	100
176	100	0^+	7972.679	10064.08	4098.60	3.6 m	0	0	100
177	101	$1/2^-$	7972.396	7922.62	4175.33	3.0 m	0	0	100
178	102	0^+	7981.911	9666.04	4563.77	5.0 m	0	0	100
179	103	$1/2^-$	7979.479	7546.65	4654.82	6.5 m	0	0	100
180	104	0^+	7987.448	9413.97	5066.10	21.5 m	0	0	100
181	105	$1/2^-$	7983.426	7259.33	5001.58	105 m	0	0	100
182	106	0^+	7989.728	9130.43	5377.07	21.84 h	0	0	100
183	107	$9/2^+$	7985.010	7126.29	5505.30	13.0 h	0	0	100
184	108	0^+	7988.699	8663.92	5734.40	0.02 %			
185	109	$1/2^-$	7981.325	6624.52	5874.09	92.95 d	0	0	100
186	110	0^+	7982.844	8263.85	6468.74	1.59 %	100	0	0
187	111	$1/2^-$	7973.791	6289.95	6579.33	1.96 %			
188	112	0^+	7973.875	7989.58	7209.70	13.24 %			
189	113	$3/2^-$	7963.011	5920.51	7258.56	16.15 %			
190	114	0^+	7962.112	7792.30	8017.69	26.26 %			
191	115	$9/2^-$	7950.576	5758.74	8050.84	14.99 d	0	100	0
192	116	0^+	7948.534	7558.40	8820.86	40.78 %			
193	117	$3/2^-$	7936.279	5583.42	9096.19	29.830 h	0	100	0
194	118	0^+	7932.033	7112.46	9490.80	6.0 y	0	100	0
195	119	$3/2^-$	7917.744	5145.72	9564	9 m	0	100	0
196	120	0^+	7912.238	6838.52	9989	34.9 m	0	100	0
197	121	$5/2^-$	7898	5101	10056	2.8 m	0	100	0
198	122	0^+	7891	6600	10624	1 m	0	100	0
199	123	$5/2^-$	7875	4718	10633	6 s	0	100	0
200	124	0^+	7868	6367		7 s	0	100	0
201	125	$1/2^-$	7851	4532		1 s	0		0
202	126	0^+	7842	5920		200 ms	0		0

Table 1 lists the main characteristics of known isotopes of osmium ($Z = 76$) taken from the AME-2012 atomic mass evaluation [2], which is in turn based on experimental data. The lightest of the bound osmium isotopes is ^{161}Os with $N = 85$, and the most heavy isotope ever observed is ^{202}Os ($N = 128$). Most of these isotopes are radioactive, but there are 5 stable isotopes: ^{187}Os, ^{188}Os, ^{189}Os, ^{190}Os, and ^{192}Os. The half-lives of ^{184}Os and ^{186}Os are, respectively, $5.6 \cdot 10^{13}$ yr and $2.0 \cdot 10^{15}$ yr, which is much longer than the age of the Universe, and, thus, they are also considered stable. Relative percentanges of the stable

isotopes in natural osmium are also shown in Table 1.

The $^{175-183}$Os isotopes decay via β^+- and electron capture ε-decays. In the $^{161-174}$Os isotopes the ε-decay competes with α-decay. As the mass number A decreases the probability of the α-decay grows and becomes almost equal to 100% in the isotopes with $A < 165$. The $^{191,193-202}$Os isotopes decay through the β^- channel.

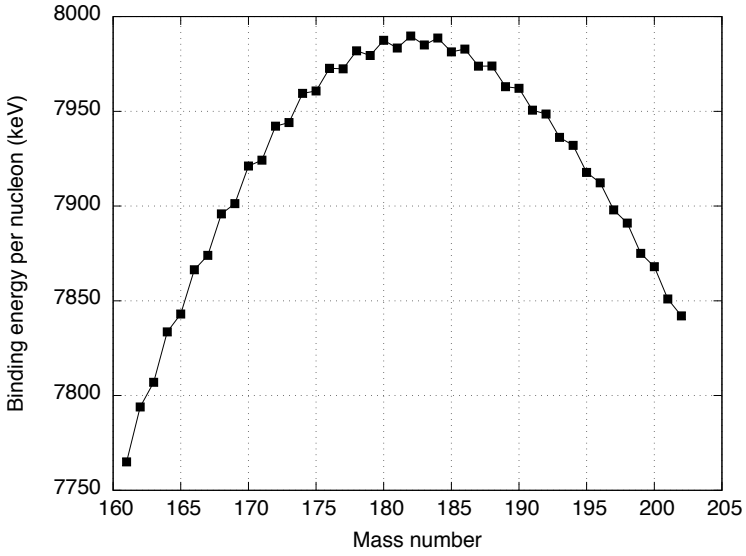

Figure 1. Per-nucleon binding energies of the known osmium isotopes.

Figures 1 and 2 show the dependence of the per-nucleon binding energy ε, neutron separation energy B_n, and proton separation energy B_p in Os isotopes on the neutron number N. The effect of pairing of neutrons within the same subshell can be clearly observed in the N-dependence of the neutron separation energies.

3. Nuclear shell model

In the above discussion of the nuclear properties it was assumed that the nucleon distribution inside of the nucleus is uniform. However, it was an unexpected discovery that the nuclear properties reveal a certain periodicity with respect to variation of the number of nucleons. The nucleons were found to be located in the nuclear shells, similarly to the atomic electrons.

The single particle nuclear shell model was proposed by M. Göppert-Mayer [3] and independently by O. Haxell, J. Jensen, and H. Suess [4]. The model was a result of systematization and generalization of a large amount of experimental data and is based on the assumption that the nuclear field V_k which interacts with the k-th nucleon is composed from three parts:

$$V_k = V_0(r) + V_1(t)(\hat{l}\hat{s}) + \sum_{i=1, i\neq k}^{N} V_{ik}(r_{ik}). \tag{4}$$

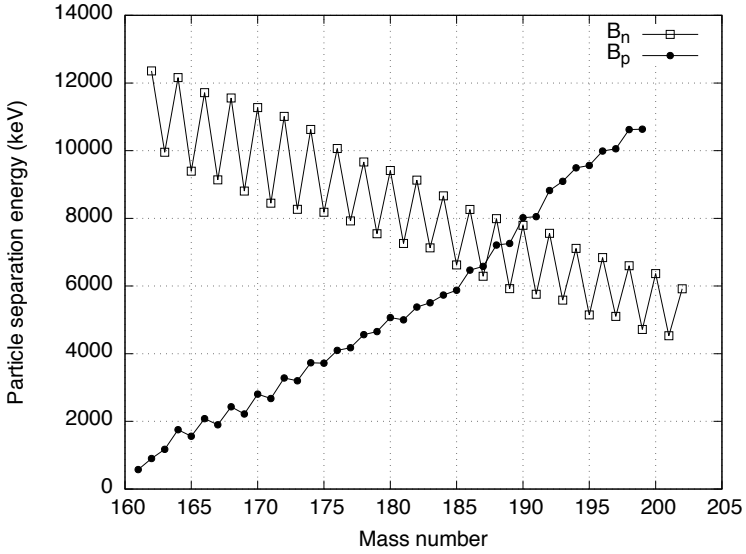

Figure 2. Particle separation energies in osmium isotopes.

The first term $V_0(r)$ describes the centrally-symmetric field, created by all the nucleons as a whole. The $V_1(t)(\hat{l}\hat{s})$ describes the spin-orbit interaction. The third term describes the residual interaction between individual nucleons in addition to the self-consistent field created by $V_0(r)$ and $V_1(t)(\hat{l}\hat{s})$.

It is important that the interaction of nucleons in the nuclear mean field leads to splitting of the levels with $j = l \pm 1/2$, where j denotes the nucleon spin and l is the orbital moment of the nucleon. The value of the spin-orbital splitting is

$$E_{j=l-1/2} - E_{j=l+1/2} = \frac{12(2l+1)}{A^{2/3}} \text{ MeV}. \tag{5}$$

The nuclear shell model leads to a sequence of single-particle states with large energy gaps at $N = 2, 8, 20, 28, 50, 82, 126$, that correspond to completely filled shells, in similaraty with inert gas atoms. Such nucleon numbers are called magic.

Within the shell model the single-particle states are described by four quantum numbers:

$$n, l, j, m,$$

where n is the principal quantum number (similar to the quantum number n that enumerates the levels of a harmonic oscillator), l is the quantum number of the orbital angular momentum, j is the quantum number of the total angular momentum, and m is the quantum number of the j's projection onto the z axis. Values of the orbital quantum number are usually represented using Latin letters:

$l = 0,$	$1, 2,$	$3, \ldots$
$s,$	$p, d,$	$f, \ldots$

The nuclear shells are sequentially filled with nucleons starting from the ground state, taking into account the Pauli principle: any vacancy with a given set of the aforementioned

four numbers can be filled by at most one nucleon of a given sort. The proton and neutron states are populated independently. The maximum number of nucleons of a given sort in the j subshell is $\nu = 2j+1$.

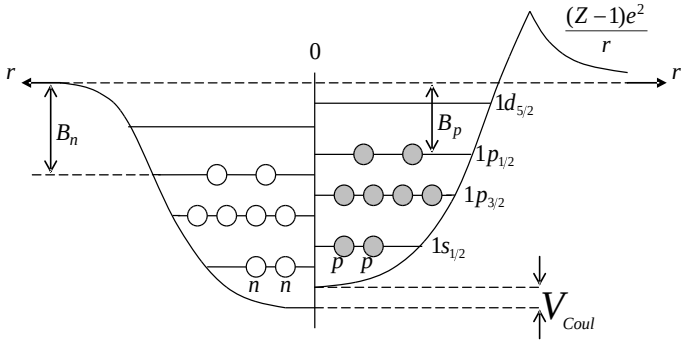

Figure 3. Proton and neutron shells in ^{16}O.

In addition to the nuclear interaction the protons in nuclei experience Coulomb repulsion. A proton is given an additional positive energy of Coulomb repulsion $\approx \frac{(Z-1)e^2}{R}$. The repulsion results in increase of the energy of the proton single-particle states and changes the potential well. Fig. 3 shows three first subshells of the single-particle shell model. This configuration corresponds to a doubly-magick ^{16}O. The Coulomb forces depend on the atomic number as $\approx Z^2$. Thus, increasing Z leads to an increase of the energy difference of the proton and neutron states and to changes of their sequence for heavy nuclei. Table 2 shows the proton and neutron level sequences for Z up to 114 and N up to 148. The second and the fourth columns show the maximum number of nucleons in the subshell.

According to this model the isotopes of osmium ($Z = 76$) have fully populated subshells up to $3s_{1/2}$ and also six protons in the $1h_{11/2}$. Neutron single particle states are populated up to the next shell ($N = 83-126$), from $1h_{9/2}$ (^{161}Os, $N = 85$) to the $3p_{1/2}$ subshell (^{202}Os, $N = 126$).

It should be noted that the nuclear shape might be in fact non-spherical, and it is very common for nuclei with several nucleons above closed shells to be deformed. In this case the energies and the relative ordering of single-particle states may change.

4. Interaction of photons with atomic nuclei

Using electromagnetic probes (that is, electron and photon beams) to study nuclear properties has a number of advantages over hadrons, since the mechanism of the energy transfer from the incident particle to the nucleus is known with a great detail. It is possible to distinguish between the effects of the interaction of a photon with a nucleus and the effects of subsequent dynamics of the resulting excited state.

An important part of photon-induced excitations are giant resonances (GR), a particular type of nuclear excitations where a large number of nucleons are involved in a collective

Table 2. Structure of single-particle nuclear shells for a spherical nucleus in the Woods-Saxon potential

Nuclear level	Z	Nuclear level	N
$1s_{1/2}$	2	$1s_{1/2}$	2
$1p_{3/2}$	6	$1p_{3/2}$	6
$1p_{1/2}$	8	$1p_{1/2}$	8
$1d_{5/2}$	14	$1d_{5/2}$	14
$2s_{1/2}$	16	$2s_{1/2}$	16
$1d_{3/2}$	20	$1d_{3/2}$	20
$1f_{7/2}$	28	$1f_{7/2}$	28
$2p_{3/2}$	32	$2p_{3/2}$	32
$1f_{5/2}$	38	$1f_{5/2}$	38
$2p_{1/2}$	40	$2p_{1/2}$	40
$1g_{9/2}$	50	$1g_{9/2}$	50
$1g_{7/2}$	58	$2d_{5/2}$	56
$2d_{5/2}$	64	$1g_{7/2}$	64
$1h_{11/2}$	76	$3s_{1/2}$	66
$2d_{3/2}$	80	$2d_{3/2}$	70
$3s_{1/2}$	82	$1h_{11/2}$	82
$1h_{9/2}$	92	$1h_{9/2}$	92
$2f_{7/2}$	100	$2f_{7/2}$	100
$1i_{13/2}$	114	$1i_{13/2}$	114
$2f_{5/2}$	120	$3p_{3/2}$	118
$3p_{3/2}$	124	$2f_{5/2}$	124
$3p_{1/2}$	126	$3p_{1/2}$	126
		$2g_{9/2}$	136
		$1i_{11/2}$	148
		$1j_{15/2}$	164
		$3p_{5/2}$	170
		$4s_{1/2}$	172
		$2g_{7/2}$	180
		$3d_{3/2}$	184

motion. The GR's are seen in the energy dependence of the reaction cross section as wide intense maxima appearing from several MeV to about 40–50 MeV.

The giant resonances can be systematized based on the angular momentum J (multipolarity) and the parity P of the initial gamma transition. The transitions with $P = (-1)^{J+1}$ are called magnetic type transitions and are denoted with "M", and those with $P = (-1)^J$ are electric transitions ("E"). Thus, E0 and M0 are electric and magnetic monopole resonances, E1 and M1 are dipole resonances, E2 and M2 correspond to quadrupole resonances and so on.

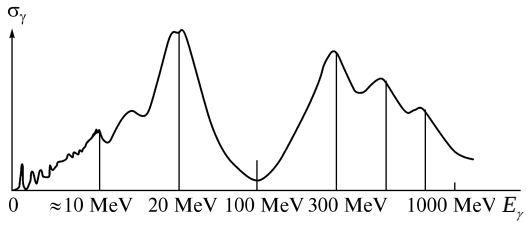

Figure 4. The cross section scheme of the γ-quanta photoabsorption by atomic nuclei in the region of γ-quanta energies of $E_\gamma < 1$ GeV.

Figure 4 shows schematically the energy dependence of photon absorption cross section. The intense maximum at about 20 MeV is a result of E1 excitation which is called the giant dipole resonance (GDR). GDR is a characteristic feature of photonuclear cross sections of all known nuclei, except for the deuteron. The energy of the maximum of the GDR depends on the mass number A and can be approximately described by the following relationship:

$$E = 80A^{-1/3}\ \text{MeV}. \tag{6}$$

The width of the GDR varies from 5 to 20 MeV for different nuclei.

The collective motion of nucleons excited in GDR is a complex state which undergoes an intricate internal dynamics from its formation to the eventual decay. Since the GDR energies excess the nucleon separation thresholds, the most probable decay channel in most nuclei is through emission of a neutron.

At higher energies (several hundred MeV) the photons are able to interact with individual nucleons. The mean free path of photons at these energies is large as compared to the size of the nucleus and they can easily penetrate deeply inside the nucleus and, hence, interact with all of the nucleons, not just the nuclear surface. The total photoabsorption cross section at these energies is proportional to the mass number A. The maximum at ≈ 300 MeV corresponds to the so-called $\Delta(1232)$ resonance or the $\Delta(1232)$-isobar, which is an intra-nucleon excitation. The width of this resonance is about 150 MeV and it quickly decays into a nucleon and a π-meson.

In the following section we consider the excited states and gamma-ray spectra of the Os isotopes.

5. Low-lying excited states of the Os isotopes

The spectrum of low-lying excited nuclear states of a doubly even ^{188}Os isotope are shown in Fig. 5.

The low-lying states are characterized with energies lower than the nucleon thresholds. Each excited stated is described by its energy, spin, parity, and isospin. In the analysis of the excited states is is possible to interpret some of the states as single-particle excitations of the nuclear shell model. In the odd isotopes of Os these are mostly neutron transitions in the $N = 83 - 126$ shell. It is a distinguishing feature of such states that there is a large spin difference and a different parity from the ground state values. In such cases long-living isomeric states can be observed, taking for example the $J^P = 3/2^-$ state at 30.814 keV in ^{189}Os. Similar states can be found in other odd isotopes of Os (table 3).

Table 3. Energies, spins-parities and half-lives of the ground and isomeric states in odd isotopes of Os

Isotope	$J^P_{\text{g.s}}$	$T^{\text{g.s}}_{1/2}$	$J^P_{\text{m.s}}$	$T^{\text{m.s}}_{1/2}$	$E^{\text{m.s}}_{\gamma}$, keV
^{191}Os	$9/2^-$	15.4 d	$3/2^-$	13.10 h	74.382
^{189}Os	$3/2^-$	stable	$9/2^-$	5.8 h	30.814
^{183}Os	$9/2^+$	13.0 h	$1/2^-$	9.9 h	170.71
^{181}Os	$1/2^-$	105 m	$7/2^-$	2.7 m	170.71

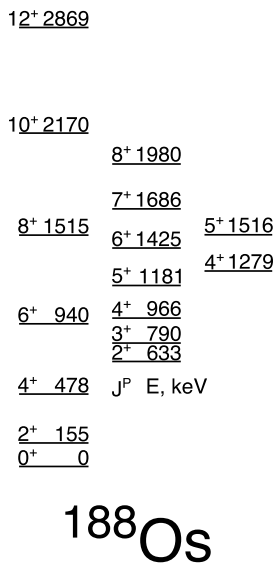

Figure 5. Low-lying excited states of ^{188}Os (data from [50]). Triaxial rotational bands built on $J = 0, 2, 4$ are shown.

In addition to single-particle excitations there are also collective excited states corresponding to rotations and surface vibrations of nuclei. Sets of excited levels of this type have the same parity, and the respective differences of spins are 2 for doubly even nuclei and 1–2 for odd nuclei.

Non-spherical doubly even nuclei in the ground state have a projection of the total angular momentum on the symmetry axis equal to zero $K = 0$. The energies of E_γ of the first excited states of such nuclei are well described by the following relationship:

$$E_\gamma = \frac{\hbar^2 J(J+1)}{2I}, \tag{7}$$

where I is the nuclear moment of inertia. Figure 6 shows energies of the first 2^+, 4^+, 6^+, 8^+, and 10^+ states in doubly even istopes $^{170-194}$Os.

It is seen from Fig. 6 that as the neutrons populate the $N = 83 - 126$ shell the energies of the levels with a given J^P first decrease, reaching the minimum value at mid-shell, and then again increase.

When $K \neq 0$ the total angular momentum J of excited states is determined by the relationship

$$J = K, K+1, K+2, \ldots, \tag{8}$$

and the rotational motion energies are described by the relationship

$$E_{\text{rot}} = \frac{\hbar^2}{2I}[J(J+1) - 2K^2]. \tag{9}$$

The sequence of excited states with these K is often called the rotational band and the level with the lowest K is the head of the rotational band. In the scheme of the excited levels

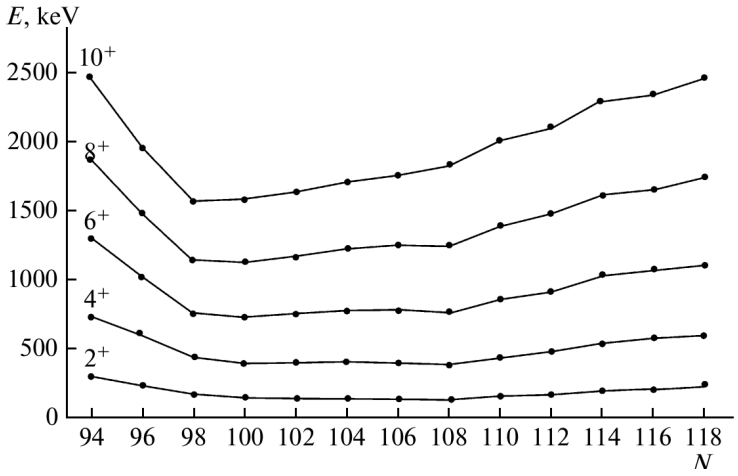

Figure 6. The spectrum of the yrast states, $0^+, 2^+, 4^+, 6^+, 8^+, 10^+$ in the even $^{170-194}$Os isotopes.

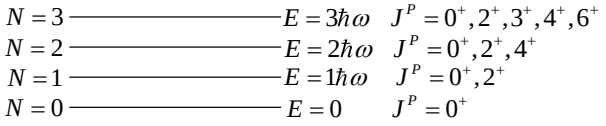

Figure 7. The spectrum of the vibrational states.

of ^{188}Os shown in Fig. 5 as an example of the rotational band the levels built up on the $J = 0, 2, 4$ are highlighted.

Like molecules the atomic nuclei also have vibrational degrees of freedom, which can be found both in spherical and deformed nuclei. The most simple of them are quadrupole vibrations $J^P = 2^+$, whose spectrum is schematically shown in Fig. 7 for the case of a doubly even nucleus with $J^P_{\text{g.s.}} = 0^+$.

N is the number of quadrupole phonons in a given excited state. The spectrum is equidistant, though in real nuclei with $N = 2, 3, \ldots$ the states split into several energy levels. The total angular momentum and parity of several quadrupole phonons is determined by the symmetry properties of the wave function describing a system of like bosons.

It is possible that in a doubly even nucleus an octupole vibration $J^P = 3^-$ is excited. The levels, corresponding to simultaneous excitation of quadrupole and octupole vibrations form a sequence $J^P = 1^-, 2^-, 3^-, \ldots$.

To the first approximation the wave function of an excited state can be expressed as a combination of different excitations

$$\psi = \psi_{\text{single}} \psi_{\text{rot}} \psi_{\text{vibr}}, \tag{10}$$

where ψ_{single} corresponds to single-particle excitations of individual nucleons of a deformed nucleus, ψ_{rot} corresponds to rotatational states with respect to different nuclear axes, and ψ_{vibr} corresponds to the vibrational degrees of freedom. Analysis of excited states of the

Os isotopes suggests complex nature of the excitations and implies coexistence of different nuclear shapes in different states.

6. Giant dipole resonance

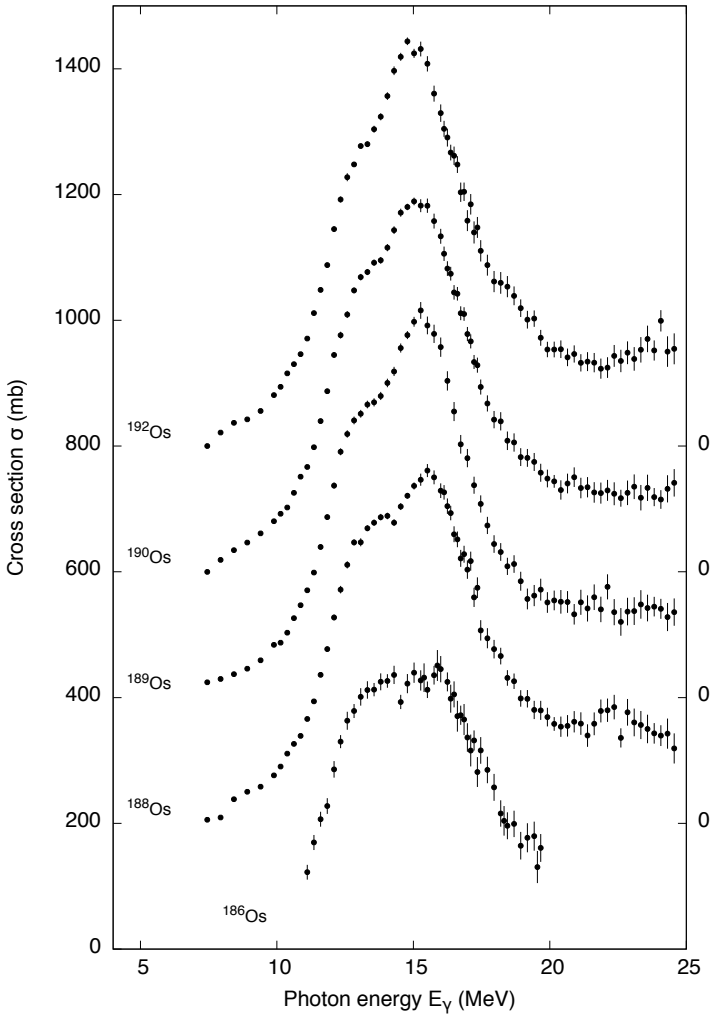

Figure 8. Cross sections of (γ, Sn) reactions on ^{186,188,189,190,192}Os.

The Giant Dipole Resonance (GDR) which was theoretically predicted by A. B. Migdal [5] and then experimentally discovered by G. Baldwin and G. Klaiber [6] is a significant factor in the physics of photonuclear reactions. The issues of formation of the GDR, its nature and decay channels were central to nuclear physics over the last 50 years.

6.1. GDR splitting in axially symmetric nuclei

The concept of deformed nuclear shells suggested by L. J. Rainwater was developed by S. G. Nilsson [7]. Energies of single-particle states were calculated by Nilsson for nucleons in a deformed axially symmetrical potential well depending on the deformation parameter β. Some configurations had minimum values of the total energy at $\beta \neq 0$, and, that is, are deformed in the ground state.

Both microscopic and macroscopic approaches treat the GDR as an excitation of a peculiar collective degree of freedom, that is, oscillations of protons with respect to the neutrons. In nonspherical axially symmetric heavy nuclei the GDR splits into two maxima, corresponding to oscillations along the a and b ellipsoid axes in the collective model, and to the difference of the energies of the particle-hole configurations in longitudinal and transverse configurations in the microscopic approach. Dipole oscillations along the greater axis of an oblong ellipsoid are characterized by smaller frequecies than oscillations in a perpendicular direction. Hence, two resonant energies of the dipole oscillations, E_a and E_b, appear in an ellipsoidally deformed nucleus.

The difference between the energies of these oscillations is

$$\Delta E = |E_a - E_b| = 80\beta A^{-1/3}\ \text{MeV}, \tag{11}$$

where $\beta = (b-a)/(r_0 A^{1/3})$ is the parameter of deformation, $r_0 = 1.3$ fm. Another form of the deformation parameter is $\beta_2 = 1.058\frac{3}{2}\frac{b^2-a^2}{b^2+2a^2}$.

At small deformations the GDR only broadens but in significantly deformed nuclei it actually splits into two distinct peaks. This effect can be illustrated by the example of photoneutron reaction cross sections shown in Fig. 9.

According to the classical collective model of GDR, the photoabsorption cross section on heavy deformed nuclei is described by superposition of two Lorentz curves as follows:

$$\sigma_{\text{abs}}(E) = \sum_{i=1}^{2} \frac{\sigma_{\text{peak}_i}}{1 + \frac{(E^2 - E_{\text{peak}_i}^2)^2}{E^2\Gamma_i^2}}, \tag{12}$$

where σ_{peak} is the peak cross section of the corresponding deformation branch of the GDR, E_{peak} is the position of the peak, Γ is the width of the peak. In collective models the ratio between cross sections of excitations along the a (major) and b (minor) axes is $1:2$.

It follows from the data in tables 4, 5 that the deformation paramter β_2 does not exceed 0.19, and, correspondingly only a single peak is seen in the photoabsorption cross section. However, the width of this peak depends both on the value of the deformation splitting $\Delta E = |E_{m1} - E_{m2}|$, and on the widths of the E_{m1} and E_{m2} states.

For isotopes of Os the I_2/I_1 ratio does not agree with the value predicted by the collective model for axially symmetric nuclei (see table 5. Experimentally measured cross sections of photonuclear reactinos on $^{186,188-190,192}$Os were obtained in [37]. The GDR peak widths are 6.0 MeV in ^{186}Os, 5.5 MeV in ^{188}Os, and about 4.8 MeV in ^{189,190,192}Os; these values are higher than what is typical for spherical nuclei. However, no splitting into two distinct peaks is observed. The Os isotopes belong to the transition region between the strongly deformed nuclei, $N \sim 100$, and the spherical nuclei, $N \sim 126$. Estimations made in [15] show that ^{186}Os has a prolate shape, ^{188}Os and ^{190}Os are asymmetric, and ^{192} is oblate shaped.

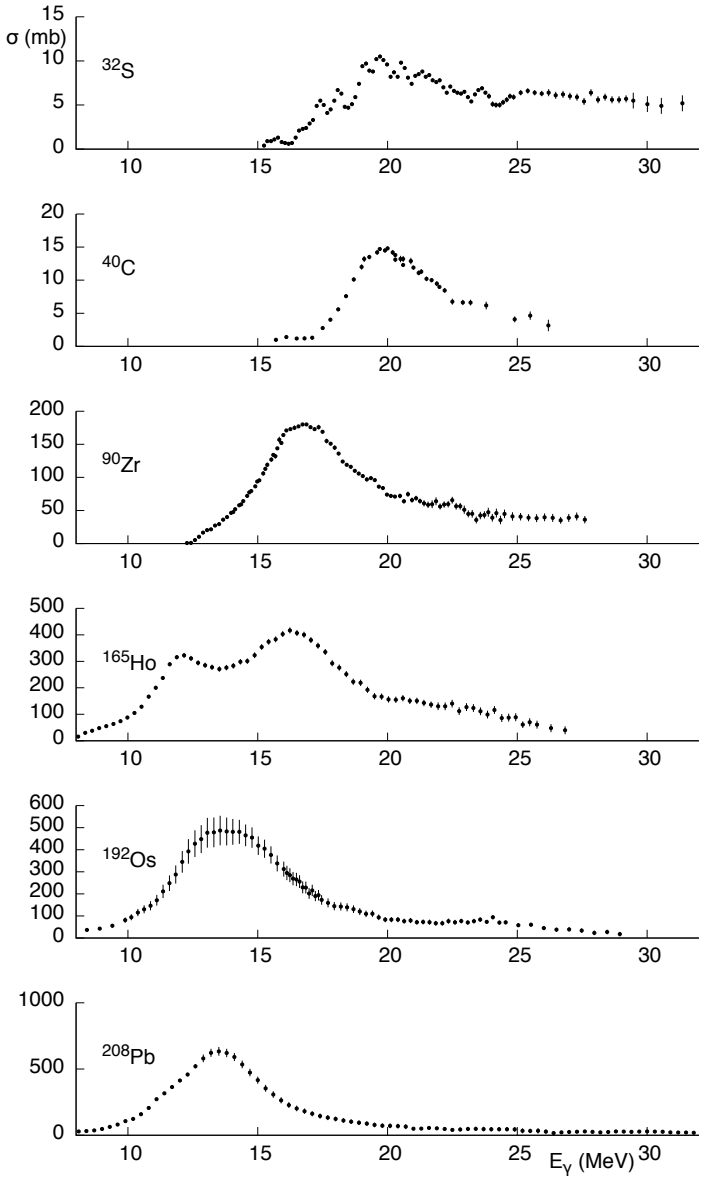

Figure 9. Cross sections of (γ, Sn) reactions on ^{32}S, ^{40}Ca, ^{90}Zr, ^{165}Ho, ^{192}Os, ^{208}Pb.

6.2. Triaxial nuclei

A prolate or oblate ellipsoidal shape is a good approximation for most medium and heavy deformed nuclei which agrees with the experimental results. However, there are exceptions to this model where a more complex triaxial shape might be needed to appropriately describe the data.

According to [37], the photoabsorption cross sections in Os can be approximated by three Lorentz curves of about the same intensity, but the peak positions of these curves do not agree with the calculations [15]. It was suggested in [16] that the Os isotopes might be

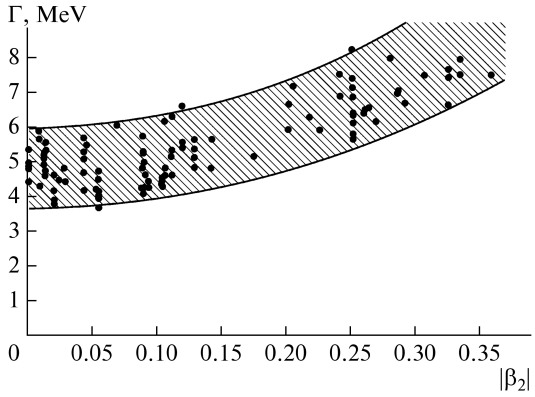

Figure 10. GDR width vs. the modulus of the nuclear quadrupole deformation parameter, $|\beta_2|$, for medium and heavy nuclei.

gamma-unstable, that is, may have a number of low-energy excited states with dramatically different nuclear shapes. The accuracy of the experimental data was insufficient to reliably identify these nuclei as either triaxial or gamma-unstable.

6.3. Effects of isospin

The isospin symmetry of nuclear interaction is a symmetry against rotations in the isospin space, that is, interchange between protons and neutrons in the system. Indeed, the experiment shows, that apart from the electromagnetic component the nuclear interaction in a pp, np, or nn system is identical. Thus, the nuclear interaction does not distinguish between neutrons and protons, and it is possible to treat both nucleons as the same particle in two distinct states. Theoretically this corresponds to two possible orientations of a $T = 1/2$ isospin vector with two projections $T_z = \pm 1/2$, the latter denoting the neutron and the former denoting the proton.

When a system of nucleons experiences rotation in the isospin space, due to the symmetry the energy levels should remain intact. The isospin symmetry is only approximate and it is violated by the electromagnetic component of the nuclear interaction, so in real nuclei with a given A only the so-called isobar analog states are kept in place, when going from one nucleus with the mass number A to another.

Effects related to the isospin quantum number are important to the photonuclear cross sections. The giant dipole resonance has an isovector nature, i.e., the absorbed photon carries $T = 1$ isospin. An isovector electric dipole $E1$ excitation leads to formation of either $T_< = T_0$ or $T_> = T_0 + 1$ branch of the GDR, where $T_0 = (N-Z)/2$ is the ground state isospin. The probabilities of formation of each branch should relate as follows [14]:

$$\frac{C^2(T_>)}{C^2(T_<)} = \frac{1}{T_0}\left(\frac{1 - 1.5T_0A^{-2/3}}{1 + 1.5A^{-2/3}}\right). \tag{13}$$

Each of the $T_<$ and $T_>$ branches corresponds to its own peak, the energy difference

Table 4. Parameters of the cross sections of the $(\gamma,sn)=(\gamma,1n)+(\gamma,2n)+(\gamma,3n)+...\approx(\gamma,\mathrm{abs})$ photoneutron reactions in the deformed nuclei. E_{mi} is the position of the GDR maximum and Γ is the GDR width. The β_2 parameters were calculated from the peak positions, E_m in accordance with formulas (1) and (2). The ratios between the axis lengths of the nucleus, b/a, obtained from β_2[8] are indicated

Chemical element	Z	N	A	E_m, MeV	Γ, MeV	β_2, [9]	β_2, [8]	β_2, [10]	$\lvert\beta_2\rvert$, [11]	b/a
Gd	64	96	160	14.7	7.5	0.33	0.3534	+0.266	0.47	1.39
Tb	65	94	159	14.7	7.6	0.41	0.326	+0.298	0.39	1.35
Ho	67	98	165	14.7	7.0	0.31	0.322	+0.306	0.33	1.35
Lu	71	104	175	14.6	6.7	0.35	0.292	+0.275	0.34	1.31
Ta	73	108	181	14.4	6.4	0.26	0.261	+0.326	0.34	1.28
W	74	112	186	14.2	6.0	0.18	0.2238	+0.185	0.22	1.24
Os	76	110	186	14.2	5.1	0.19	0.19026	+0.182		1.20
Os	76	112	188	14.2	5.2	0.18	0.18009	+0.172		1.19
Os	76	113	189	14.0	4.9	0.18	0.17596	+0.165		1.18
Os	76	114	190	14.0	4.8	0.15	0.15217	+0.156		1.16
Os	76	116	192	14.0	4.8	0.15	0.14789	+0.142		1.15
Pt	78	116	194	13.8	4.8		0.1434	+0.14	0.08	1.15
Pt	78	117	195	14.0	4.8	0.17			0.11	
Pt	78	118	196	13.8	4.4		0.1308	+0.131	0.05	1.13
Pt	78	120	198	13.7	4.6		0.113	+0.084	0.03	1.12

between the peak centers being

$$E(T_>)-E(T_<)=60\frac{T_0+1}{A}\ \mathrm{MeV}. \tag{14}$$

In heavy nuclei the amount of this splitting can be as high as 10–12 MeV.

The scheme of the isospin splitting of the GDR is shown in Fig. 11. Isospin conservation law results in selection rules for outgoing nucleons, and specifically inhibits emission of neutrons from the $T_>$ branch, which leads to increased yield of protons. Indeed, this effect is seen in practice as a much higher cross section of photoproton reactions, compared to the prediction of statistical model calculations.

7. Combined model of photonuclear reactions

Following the Bohr's concept of compound nucleus [17] it is assumed in the combined model of photonuclear reactions (CMPNR) that the nuclear reaction can be approximately divided into two independent stages: formation of a compound system after absorption of a photon and a subsequent decay of this system into reaction products. In addition to this it is also assumed that in the mass range from $A\approx 40$ to transuranic elements one can take into consideration only three competing decay channels of the compound system: emission of a neutron, a proton, or a photon.

Thus, in order to describe different photonucleon reactions, that take place after absorption of a photon with the energy E_γ, one has to: (1) calculate the photoabsorption cross

Table 5. Parameters of the components of deformation GDR splitting in nuclei with an occupied neutron shell N(82–126) [12]. E_{mi} is the position of the component maximum; σ_{mi} is the cross section value of the component in the maximum; Γ_i is the width of the component. I_2/I_1 is the ratio between the integral cross section components of deformation splitting

Chemical element	Z	N	A	E_{m1}, MeV	σ_{m1}, mb	Γ_1, MeV	E_{m2}, MeV	σ_{m2}, mb	Γ_2, MeV	I_2/I_1
Gd	64	96	160	12.23	215	2.77	15.96	233	5.28	2.07
Tb	65	94	159	12.07	196	2.98	15.88	248	5.1	2.17
Ho	67	98	165	12.28	214	2.57	15.78	246	5	2.30
Lu	71	104	175	12.32	217	2.5	15.47	287	4.7	2.49
Ta	73	108	181	12.3	259	2.43	15.23	341	4.48	2.43
W	74	112	186	12.59	211	2.29	14.68	334	5.18	3.58
Os	76	110	186	13.03	308	3.13	15.26	302	3.38	1.06
Os	76	112	188	12.81	260	2.76	14.88	390	4.19	2.28
Os	76	113	189	12.68	268	2.71	14.68	395	3.62	1.97
Os	76	114	190	12.68	206	2.6	14.4	401	4.16	3.11
Os	76	116	192	12.68	206	2.49	14.35	389	4.41	3.34
Pt	78	117	195	13.04	386	3.13	15.04	228	4.6	0.87

Table 6. Parameters of the isospin splitting of the GDR in isotopes of Os

Isotope	N	T_0	$E(T_>) - E(T_<)$, MeV	$c^2(T_>)/c^2(T_<)$
^{166}Os	80	7	2.9	1.13
^{180}Os	104	14	5.0	0.31
^{186}Os	110	17	5.8	0.17
^{192}Os	116	20	6.6	0.07
^{196}Os	120	22	7.0	0.02

section; (2) loop over every possible or, at least, every important process of emission of nucleons and photons at the given excitation energy of the target nucleus.

7.1. Photoabsorption cross section

Neglecting effects near the threshold, the total photoabsorption cross section can be represented as a sum of several Lorentz curves, that approximate the strength functions of the giant resonances excited when $E_\gamma < 40$ MeV and the quasideutron photon absorption cross section [18], which dominate at around $40 < E_\gamma < 140$ MeV.

The model considers three giant resonances: the giant dipole resonance (GDR), the giant quadrupole resonance (GQR), and the giant dipole resonance overtone. The resonance energies and integral cross sections (with exchange current corrections) are calculated using the semi-microscopic model of oscillations described in [38, 19, 20]. There are only two free parameters in the model: the excitation energy and the ground state parameter of deformation. These parameters can be extracted from the experimental data and a simple semi-empirical formula was obtained for the GDR, allowing to estimate the excitation energy within the accuracy of ≤ 0.2 MeV [21]. Also in the same work a rather reliable

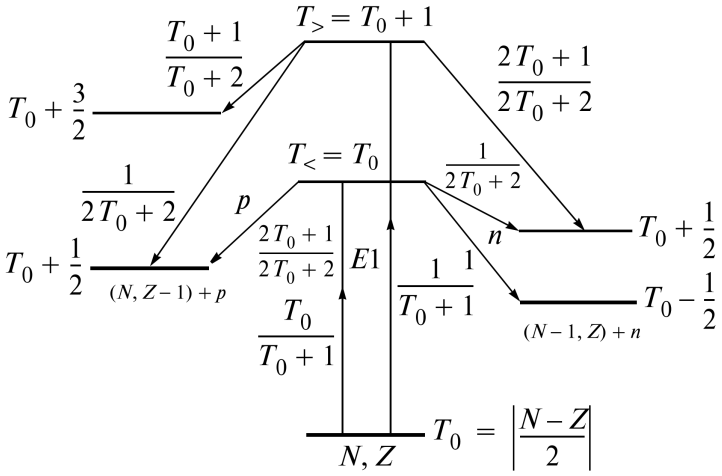

Figure 11. The isospin scheme of the excitation and decay of $T_<$ and $T_>$ of the states of the dipole giant resonance of the nucleus (N,Z). The relative probabilities of the excitation and decay are indicated

expression that can be used to estimate the width of the GDR was obtained from analysis of experimental data. The exciton model was used to estimate the widths of other resonances.

The quasideutron cross section parameters were taken the same as in Ref. [22].

7.2. Emission of particles

To describe the particle emission processes the CMPNR model uses a combination of the exciton model and the Weisskopf-Evin evaporation model [23]. Usage of semi-classical statistical models to describe the photonuclear reactions in the energy range $E \leq 30$ MeV causes certain difficulties due to the fact that the doorway state in this case is a significantly collective dipole excitation, a coherent superposition of different $1p1h$ excitations, which is often neglected. However, this leads to serious errors in estimates of photoneutron and photoproton yields and their respective energies.

The CMPNR model [23] accounts for two aspects of this problem: (a) the effect of the isospin splitting of the GDR on the photoproton yield and (b) the effect of the structure of the GDR on semi-direct reactions.

7.2.1. Isospin effects

The nuclear isospin is taken into account only during decay of the GDR. For each intermediate state Z,N only two isospin values are considered: $|N-Z|/2$ and $|N-Z|/2+1$, since the GDR lies at relatively low excitation energies.

To take into account the isospin quantum number a certain correction is needed in the expressions describing the nucleon emission rate in the excited state of a pre-equilibrium or equilibrium nucleus: the rate of decay of the $|E,T\rangle_i$ initial state into the $|E',T'\rangle_f$ final state through emission of a nucleon of a type $k = \pi, \nu$ (a proton or a neutron) with the energy ε

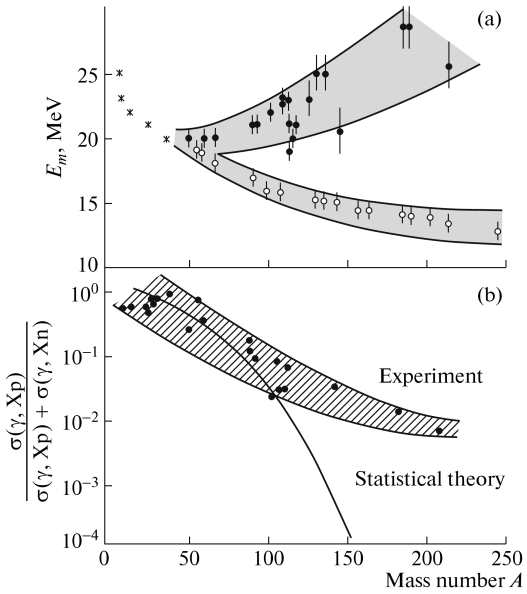

Figure 12. (a) The energy of the cross section maxima of the photoproton (γ, Xp) (dark dots) and photoneutron (γ, Xn) (open circles) of the reactions depending on A. At $A < 50$ the maxima of these cross sections coincide. (b) The experimental dependencies and the dependencies predicted by statistical theory on A of the relative contribution of the cross sections of the photoproton reactions to the total cross section of the γ-quantum absorption

can be calculated using the relationship

$$\lambda_k(\varepsilon, E, T \to T') = \frac{2s+1}{\pi^2\hbar^3}\mu\varepsilon\sigma_k(\varepsilon)\frac{\omega_f(E', T')}{\omega_i(E)}p(T' \to T), \tag{15}$$

where $T = T_0, T_0 + 1$, $T' = T_0', T_0' + 1$ (T_0 and T_0' are the initial and final ground state isospins), $s = 1/2$ is the nucleon spin, μ is its reduced mass, $\sigma_k(\varepsilon)$ is the inverse reaction cross section, $\omega_i(E) = \omega_i(E, T_0) + \omega_i(E, T_0 + 1)$ is the total level density of the initial nucleus at the excitation energy E, $\omega_f(E', T')$ is the level density of the final nucleus with the isospin T' at the excitation energy $E' = E - B_k - \varepsilon$ (B_k is nucleon separation energy for nucleon type k) and

$$p(T' \to T) = \tag{16}$$
$$\frac{\omega_f(E', T')\langle T', T_{0Z} - t_{zk}, \frac{1}{2}, t_{zk} | T, T_{0Z}\rangle^2}{\omega_f(E', T_0')\langle T_0', T_{0Z} - t_{zk}, \frac{1}{2}, t_{zk} | T, T_{0Z}\rangle^2 + \omega_f(E', T_0' + 1)\langle T_0' + 1, T_{0Z} - t_{zk}, \frac{1}{2}, t_{zk} | T, T_{0Z}\rangle^2}$$

is the factor describing the fraction of the $|E, T\rangle_i$ states populated in $T' \to T$ transitions (T_{0Z} is the isospin projection of the initial nucleus and t_{zk} is the isospin projection of the outgoing nucleon).

The level densities of heavy nuclei can be approximated with the expressions $\omega_f(E', T_0') \approx \omega_f(E')$ and $\omega_f(E', T_0' + 1) \approx \omega_f(E' - \Delta_1')$, where Δ_1' is the energy of the first excited state with the isospin $T_0' + 1$ in the final nucleus.

7.2.2. Effect of the structure of the GDR on semi-direct reactions

Semi-direct reaction channel corresponds to emission of a nucleon from the doorway $1p1h$ state. It is assumed by the exciton model that all $1p1h$ configurations at a given excitation energy are populated with the same probability and the effect of the orbital (l) and the total (j) angular moments of the excited nucleon on its ability to exit from target nucleus is neglected, which results in incorrect description of the semi-direct photonuclear reactions.

Within the shell model the doorway state of an axially symmetric nucleus is treated as a coherent superposition of $1p1h$ states $|\alpha,\beta^{-1}\rangle$, where $|\alpha\rangle = \sum_{lj\in\alpha} c_{lj}|nljm\rangle$ and $|\beta\rangle$ are single-particle states with a total angular momentum projection m, e.g., in the Nilsson potential ($|nljm\rangle$ denotes eigenstates of a spherical harmonic oscillator).

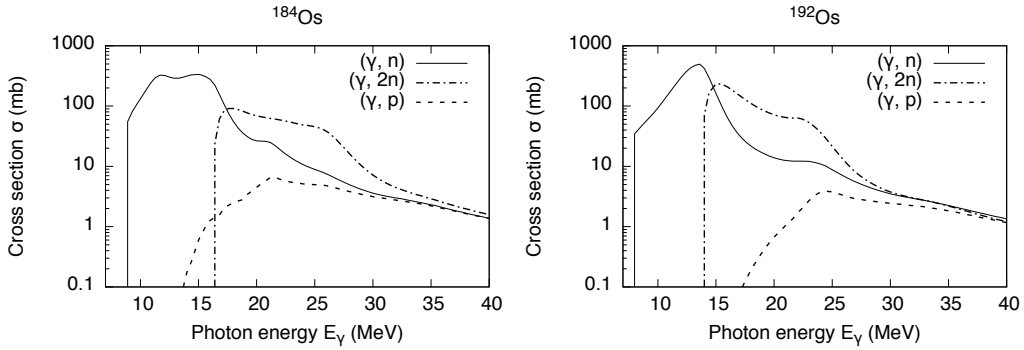

Figure 13. Cross sections of the (γ, 1n), (γ, 2n), and (γ, 1p) reactions on ^{184,192}Os calculated using the CMPNR model.

The decay rate of a doorway dipole state at the energy E with outgoing nucleon with the energy ε can be expressed as

$$\lambda(\varepsilon,E) = \sum_{\alpha\beta^{-1}} P_{\alpha\beta^{-1}} \sum_{lj\in\alpha} c_{lj}^2 \lambda(\alpha\beta^{-1},E;\varepsilon ljm), \tag{17}$$

where $P_{\alpha\beta^{-1}}$ is the relative probability of dipole excitation of the $|\alpha\beta^{-1}\rangle$ configuration, which is proportional to the squared matrix element of a single-particle $E1$ transition $\langle\alpha|2t_z rY_{1M}(\hat{\mathbf{r}})|\beta\rangle^2$ (the sum of such probabilities over all nucleon transitions should be equal to 1);

$$\lambda(\alpha\beta^{-1},E;\varepsilon ljm) = \frac{2s+1}{\pi^2\hbar^3}\mu\varepsilon\sigma_{ljm}(\varepsilon)\frac{\omega(\beta^{-1},E')}{\omega(\beta^{-1},ljm;E)} \tag{18}$$

is the probability of decay per unit time of a $|\alpha\beta^{-1},E\rangle$ configuration with an outgoing εljm nucleon, $\sigma_{ljm}(\varepsilon) = \frac{1}{2}\pi\lambda\!\!\!^{-2}T_{jl}(\varepsilon)$ is the cross section of the capture inverse reaction for a εljm nucleon ($T_{jl}(\varepsilon)$ is the transmission coefficient fo a nucleon with the orbital l and total j angular moments), $\omega(\beta^{-1},E'$ is the β^{-1} hole level density around the energy $\varepsilon_{\beta^{-1}}$ ($E' = E-B-\varepsilon$),

$$\omega(\beta^{-1},ljm;E) = \int_0^{E-B} \omega_{ljm}(\varepsilon)\omega(\beta^{-1},E-B-\varepsilon)\,d\varepsilon \tag{19}$$

is the total density of the $|\beta^{-1}, ljm\rangle$ configurations with given quantum numbers βljm at the energy E, and $\omega_{ljm}(\varepsilon)$ is the total density of the ljm states to which a nucleon with the energy ε can be captured.

Calculations (e.g., using the Nilsson potential) show that the number of single-particle levels with the fixed quantum numbers ljm increases linearly with the increase of the particle excitation energy: $N_{lj} = a_{lj} + g_{lj}\varepsilon$, so the single-particle level densities $\omega_{ljm}(\varepsilon) = \frac{N_{lj}(\varepsilon)}{d\varepsilon}$ can be approximated with the g_{lj} constants. The hole level density $\omega(\beta^{-1}, E')$ which is used in (18) and (19) can be appriximated with a Breit-Wigner's curve, normalized to unity over the interval $0 \leq E' \leq \infty$ with the width estimated using the optical model.

Figure 13 shows as an example the cross sections of the (γ, 1n), (γ, 2n), and (γ, 1p) reactions on ^{184,192}Os calculated using the CMPNR model.

8. Evaluated cross sections of photoneutron reactions

Data on partial photoneutron reactions, primarily (γ, 1n), (γ, 2n) and (γ, 3n), are widely used in both basic and applied research. There are investigations of Giant Dipole Resonance (GDR) features and mechanisms of its both excitation and decay (configurational and isospin splitting, competition between statistical and direct processes in GDR decay channels, sum rule exhaustion, etc), monitoring of the beam luminosity in ultrarelativistic heavyion colliders and various problems of astrophysics. Many data, first of all cross sections, for partial reactions together with those for total reactions were obtained using various γquanta sources as a rule many years ago and were included into various reviews [24], Atlases [25, 26] and databases [27].

The main problem of photonuclear experiments is the absence of intensive beams of monoenergetic photons. Therefore various methods for creation special conditions in which the effective photon energy spectrum in any approach can be interpreted as similar to the monoenergetic one (as whole looks like monoenergetic) are used.

In experiments with bremsstrahlung beams the mathematical method is used. At the first step the reaction yield $Y(E_m)$ — folding of cross section with continuous energy photon spectrum of bremsstrahlung

$$Y(E_m) = \alpha \int_{E_{\text{th}}}^{E_m} W(E_m, E)\sigma(E)\, dE, \tag{20}$$

where dependent on photon energy cross section $\sigma(E)$ of reaction with threshold E_{th} is folded with photon spectrum $W(E_m, E)$ with endpoint energy E_m is measured. After that one of many well-known mathematical methods could be used for reaction cross section obtaining (unfolding) from the yield. Those are constructed by such a manner that the needed result—reaction cross section—could be obtained for effective photon spectrum (experiment apparatus function) looks as quasimonoenergetic (close to Gaussian) line. Because of that the cross section wanted is really definitely localized and its resolution is near to the width of apparatus function line constructed. Majority of such kind experiments were carried out using bremsstrahlung beams from electron betatrons—at Russia, USA, Australia [26].

The alternative method of direct cross section measuring is using of quasimonoenergetic photons obtained by annihilation in flight of relativistic positrons. The idea is to avoid unfolding procedure mentioned above because annihilation line has arbitrary small (about several hundreds keV) width. But because positron annihilation photons are accompanied by positron bremsstrahlung difference procedure should be used - two experiments with positrons and electrons are combined to take into account bremsstrahlung from positrons

$$Y_{e^+}(E_j,E) - Y_{e^-}(E_j,E) = Y(E_j,E) \approx \sigma(E). \tag{21}$$

The effective photon spectrum (Fig. 14) obtained by correspondent subtraction is close to quasimonoenergetic with the energy resolution equal to annihilation line width. Majority such kind experiments were been carried out using linear accelerators at the National Lawrence Livermore Laboratory (USA), France Centre dEtudes Nucleaires de Saclay and some other laboratories using. Near all results of those experiments have been published in [25].

One can see that experimental methods used for photonuclear reaction cross section obtaining were quite different in general. Additionally the methods for obtaining partial photonuclear, primarily photoneutron, reactions also differ significantly.

In bremsstrahlung experiments data under discussion were obtained using the method of outgoing neutron detection where the summed photoneutron yield cross section

$$\sigma(\gamma,Sn) = \sigma[(\gamma,1n) + 2(\gamma,2n) + 3(\gamma,3n) + \ldots] \tag{22}$$

is measured directly. Since the neutron from the (γ, 1n) reaction is detected once, two neutrons from the (γ, 2n) reaction are detected twice, and so on, the cross sections of partial reactions appear in $\sigma(\gamma$, Sn) with corresponding multiplicity factors. Therefore, to decompose $\sigma(\gamma$, Sn) into partial reactions one need to know which reaction produced the detected neutron. This is a wellknown problem of neutron multiplicity sorting.

Corrections of $\sigma(\gamma$, Sn) for neutron multiplicity in bremsstrahlung experiments can be done using nucleus statistical theory model giving to one possibility to obtain total (unweighted) photoneutron reaction cross section

$$\sigma(\gamma,tot) = \sigma[(\gamma,1n) + (\gamma,2n) + (\gamma,3n) + \ldots]. \tag{23}$$

After that partial reaction cross section could be obtained by using correspondent subtraction procedures, for example, till the threshold B_{3n} of the reaction (γ, 3n)

$$\sigma(\gamma,2n) = \sigma(\gamma,Sn) - \sigma(\gamma,tot). \tag{24}$$

The most widely used experimental method for separation of reactions with various numbers of outgoing neutrons used both at Livermore and Saclay was neutron multiplicity sorting. That was based on main supposition that both neutrons from (γ, 2n) reaction have kinetic energy smaller than unique one neutron from reaction (γ, 1n) has. To measure neutron kinetic energy quite different methods were used—so called “ringratio” method (concentric rings of BF_3-counters embedded into paraffin or polyethylene) at Livermore and specially calibrated large Gdloaded liquid scintillator at Saclay [24, 25]. Those arrangement differences mean that cross section obtaining conditions were different. That

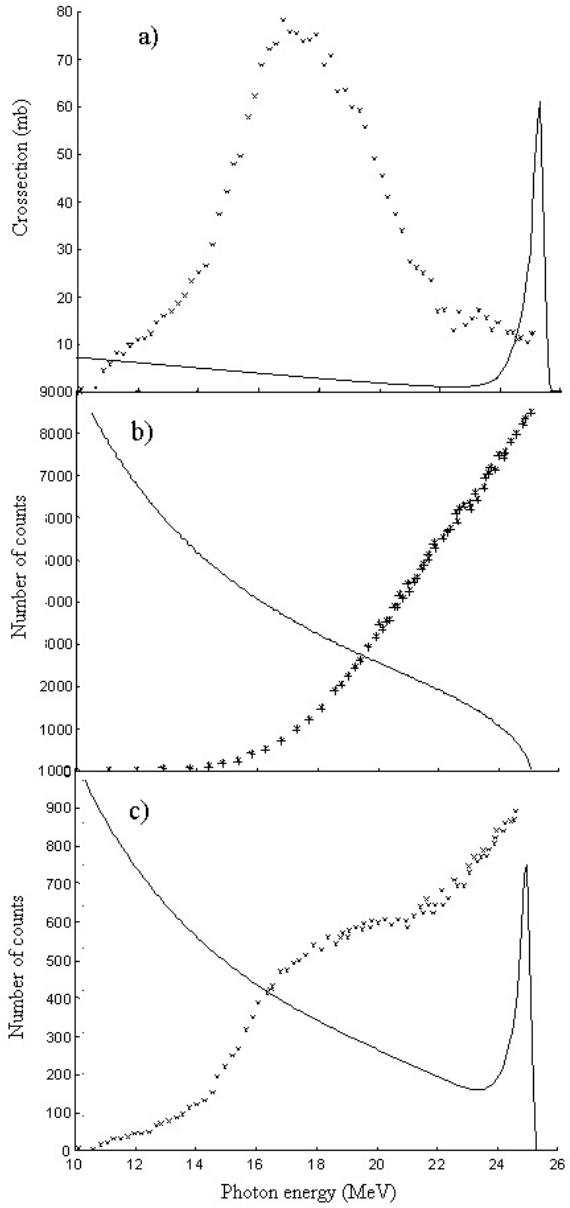

Figure 14. Explanation of the idea of experiment using annihilation photons (crosses - experimental results, lines - effective photon spectra): a) cross section of the reaction $\sigma(E)Y_{e^+}(E_j) - Y_{e^-}(E_j) = Y(E_j)$; b) yield $Y_{e^-}(E_j)$ of the reaction with electrons; c) yield $Y_{e^+}(E_j)$ of the reaction with positrons.

resulted in many complex discrepancies between partial photoneutron reaction cross sections obtained both at Livermore and Saclay. Generally and briefly—(γ, 1n) reaction cross sections are larger at Saclay but all (γ, 2n) ones—vise versa at Livermore and those disagreement are very large (till 100%). The reasons of various disagreements mentioned above and methods for their overcoming were the subjects of special investigations during

many years [28, 29, 30, 31, 32]. Studying data on the cross sections of partial photoneutron reactions revealed that many data obtained using various experimental techniques for neutron multiplicity sorting contain significant systematic errors that can be attributed to ambiguous determination of the multiplicity of the detected neutrons.

In recent studying [33, 34, 35] the special criteria for systematic uncertainties, transition multiplicity functions

$$F_i = \sigma(\gamma,in)/\sigma(\gamma,Sn) = \sigma(\gamma,in)/\sigma[(\gamma,1n)+2(\gamma,2n)+3(\gamma,3n)+\ldots] \qquad (25)$$

assume values in excess of those physically admissible (1.00, 0.50, 0.33, ...for $i = 1,2,3,\ldots$, respectively). The regions where F_i function values exceeding the indicated limiting values are observed for the cross sections of reactions with a certain multiplicity it also display physically forbidden negative values in the cross sections of reactions with different multiplicities.

Photodisintegration of ^{190}Os was investigated using beams of bremsstrahlung [36]: $\sigma(\gamma$, Sn) (3) was obtained and used for estimating $\sigma(\gamma$, tot) by statistical theory correction.

Photodisintegration of various Osmium isotopes was investigated using quasimonoenergetic photons from annihilation in flight of relativistic positrons [37].

In experiments with annihilation photons using so-called "ring-ratio" method for neutron multiplicity sorting [26, 27] (γ, 1n) and (γ, 2n) reactions cross sections for ^{186}Os and (γ, 1n), (γ, 2n) and (γ, 3n) reactions cross sections for isotopes ^{188,189,190,192}Os were obtained at Livermore [37]. Various partial reaction cross sections were used for determination of the total photoneutron reaction (γ, tot) (4) and neutron yield reaction (γ, Sn) (3) cross sections.

Experimental data for ^{186,188,189,190,192}Os isotopes [37] included into EXFOR-database [27] are presented in Figs. 15–19.

Typical example (^{192}Os) of correspondent data $F_i^{\rm exp}$ (6) is presented in Fig. 20 together with the results $F_i^{\rm theor}$ calculated in the frame of combined model of photonuclear reactions [38, 39, 40]. Analogous data were obtained for ^{186,188,189,190}Os isotopes (those for ^{188,189}Os were published in [41]. One can see in Fig. 20 that in energy range $E_\gamma \sim 16.5-21.5$ MeV $F_i^{\rm exp} < 0$ and $F_2^{\rm exp} > 0.50$: because of significant systematic uncertainties of neutron multiplicity sorting some amount of neutrons were erroneously transmitted from $\sigma(\gamma$, 1n) into $\sigma(\gamma$, 2n) and therefore data for cross sections of reactions with multiplicities "1" and "2" are not reliable. Additionally one can see that for energy range $E_\gamma >\sim 26$ MeV $F_i^{\rm exp} < 0$ and $F_3^{\rm exp} > 0.33$. It means that in this energy region data for cross sections of reactions with multiplicities "1" and "3" also are not reliable. Generally similar situations existed in case of each investigated Os isotopes differ from one to one by concrete energy ranges and pairs of multiplicity mixed—"1—2", "1—3", "2—3".

An experimentallytheoretical approach for evaluating cross sections that are free of the shortcomings of experimental neutron multiplicity sorting was proposed in [42, 43] for obtaining data on the cross sections of partial photoneutron reactions that would be free from the indicated systematic errors. The approach was based on using data on the neutron yield reaction cross section $\sigma(\gamma$, Sn) (3) that is not subjected to the neutron multiplicity sorting problem as the initial experimental data. $\sigma(\gamma$, Sn) is divided into the cross sections of partial reactions with the aid of calculations performed using a well-tested combined model of photonuclear reactions [38, 39, 40]. If this approach is used, the cross sections of partial reactions σeval(γ, in) are evaluated by combined using of the calculated transition

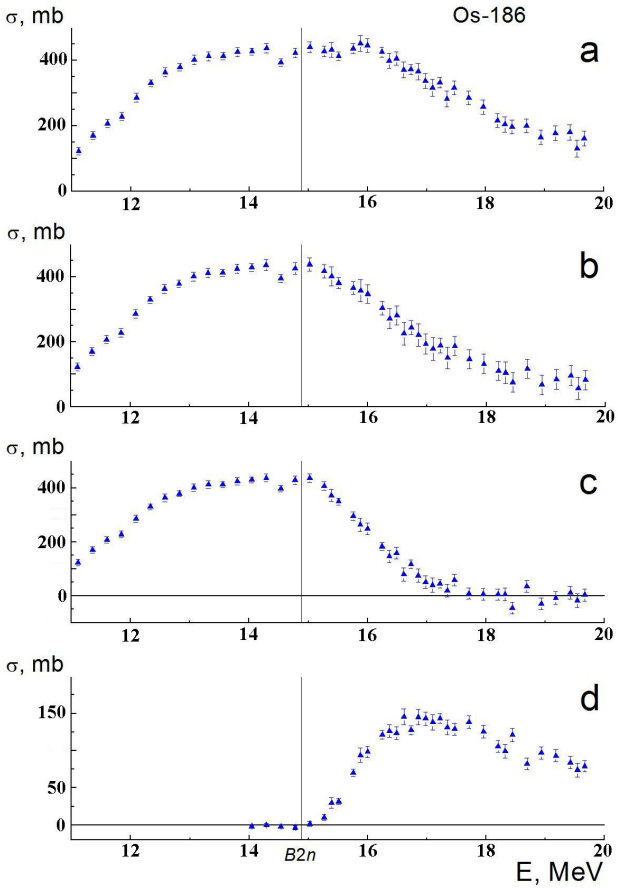

Figure 15. Experimental data [37] for ^{186}Os: a- $\sigma(\gamma, \mathrm{Sn})$, b- $\sigma(\gamma, \mathrm{tot})$, c- $\sigma(\gamma, 1\mathrm{n})$, d- $\sigma(\gamma, 2\mathrm{n})$.

functions and the experimental data on the cross section of the photoneutron yield reaction $\sigma\exp(\gamma, \mathrm{Sn})$:

$$\sigma_{\mathrm{eval}}(\gamma, in) = F_i^{\mathrm{theor}} \sigma_{\mathrm{exp}}(\gamma, Sn). \tag{26}$$

Evaluated cross sections of partial reactions (γ, 1n), (γ, 2n), and (γ, 3n) were used for obtaining new data for total photoneutron reaction cross sections (1) similar to those for the number of medium and heavy nuclei [33, 34, 35, 41, 42, 43].The evaluated cross sections for total and partial reaction cross sections for the same isotope ^{192}Os are presented in Fig. 21 in comparison with experimental data [37]. Analogous data were evaluated for ^{186,188,189,190}Os isotopes (those for ^{188,189}Os were published in [41]).

One can see that the deviations of evaluated data from experimental ones are noticeably large. Correspondent integrated cross sections are presented in the Table 7. One can see that deviations under discussion are individual for each isotope. If for ^{186,190}Os those are not so large, for ^{188,190,192}Os those are significant. The disagreements between experimental and evaluated cross sections can be attributed to that that the kinetic energy of neutrons determined in experiment [24] corresponds to their multiplicity less directly than was as-

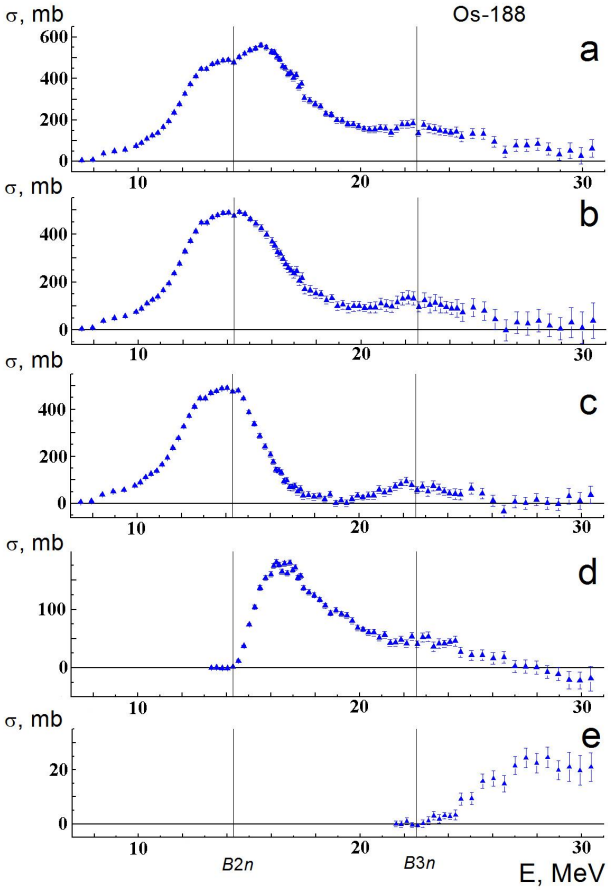

Figure 16. Experimental data [37] for ^{188}Os: a- $\sigma(\gamma, \mathrm{Sn})$, b- $\sigma(\gamma, \mathrm{tot})$, c- $\sigma(\gamma, 1\mathrm{n})$, d- $\sigma(\gamma, 2\mathrm{n})$, e- $\sigma(\gamma, 3\mathrm{n})$.

sumed in the method of neutron sorting that was used and directly depends on real energy spectra of emitted neutrons. The neutron multiplicity sorting method used is based on the assumption that alone neutron from the $(\gamma, 1\mathrm{n})$ reaction has a much higher energy than both neutrons from the $(\gamma, 2\mathrm{n})$ reaction. However, experimental and theoretical studies [44, 45] of the spectra of neutrons from reactions $(\gamma, 1\mathrm{n})$, $(\gamma, 2\mathrm{n})$, and $(\gamma, 3\mathrm{n})$ suggest that the ratios between the spectra of neutrons emitted in these reactions do not coincide with that the principal assumption.

Therefore the systematic errors in sorting neutrons with multiplicities 1 and 2 and/or 2 and 3 and/or 1 and 3 are associated with the redistribution of neutrons among the 1n, 2n, and 3n channels. This redistribution could be due [45] to the similarity between kinetic energies of neutrons from different partial reactions, meaning that the use of the neutron multiplicity sorting technique described in [24] cannot be justified for Os isotopes as well as for many others studied before [33, 34, 35, 43, 44, 45]. Because many experimental data for partial photoneutron reaction cross sections were obtained with noticeable systematic errors they are not reliable in reality and therefore a significant part of experimental data under discussion should be re-analyzed and/or re-evaluated and moreover re-measured using

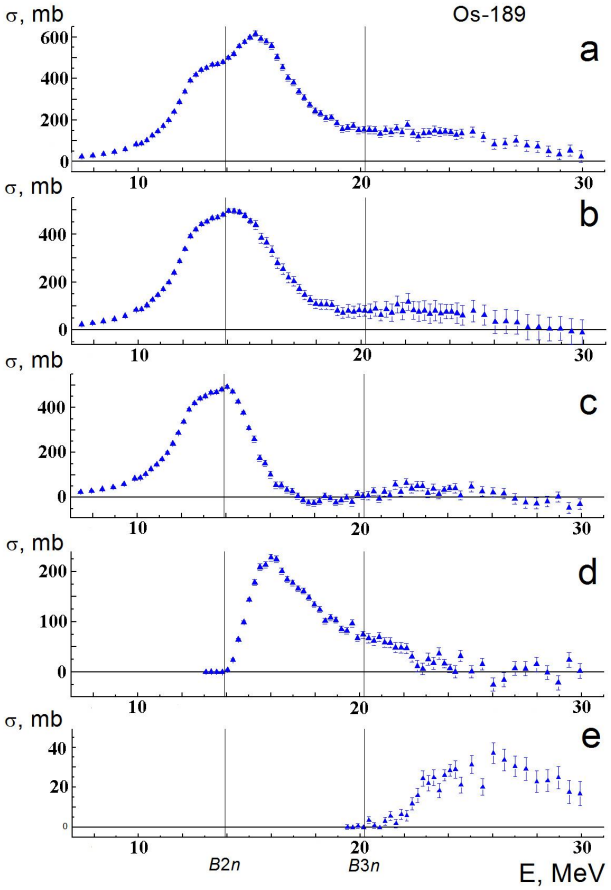

Figure 17. Experimental data [37] for ^{189}Os: the same as in Fig. 16.

advance methods free of shortcomings of neutron multiplicity sorting.

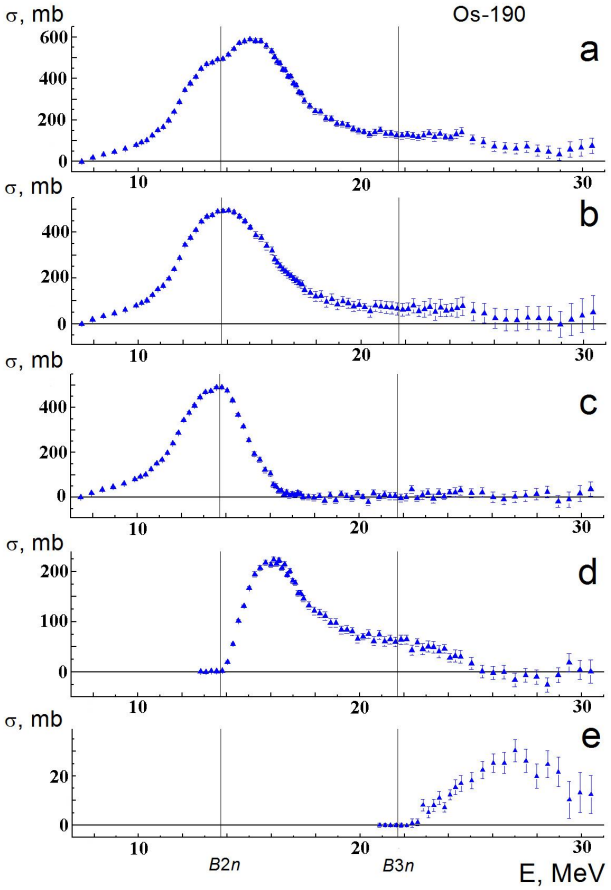

Figure 18. Experimental data [37] for ^{190}Os: the same as in Fig. 16.

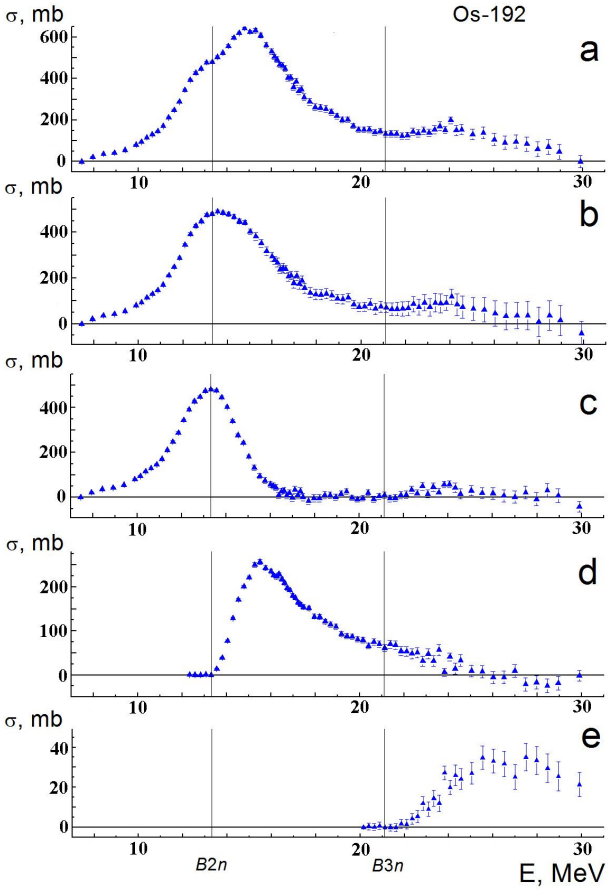

Figure 19. Experimental data [37] for ^{192}Os: the same as in Fig. 16.

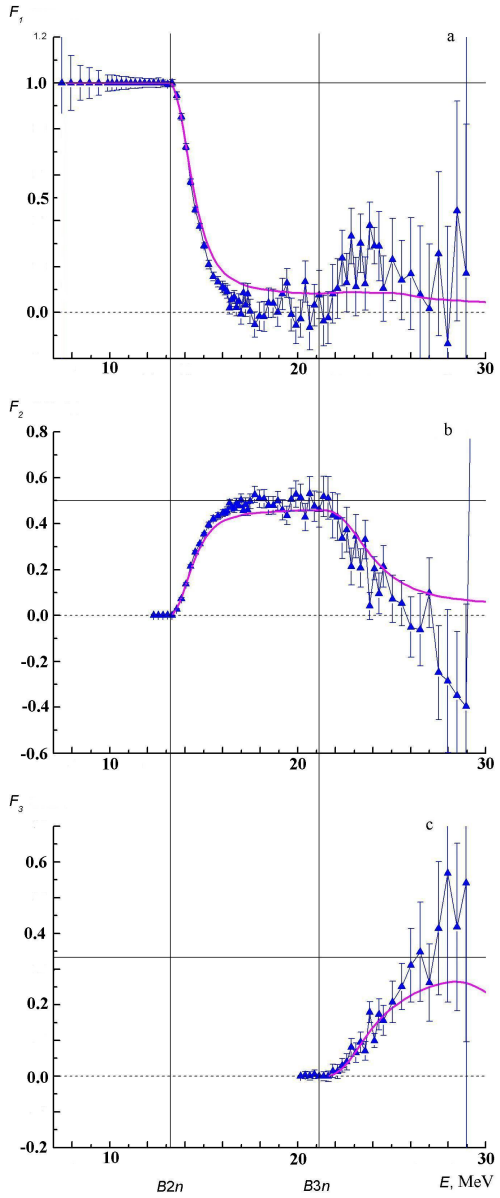

Figure 20. Comparison (from top to bottom) of ratios $F^{\mathrm{exp}}_{1,2,3}$ (3), obtained using experimental data (triangles, [37]), with F_i^{theor}, obtained using combined model [38, 39, 40] for isotope ^{192}Os. B_{2n} and B_{3n} are the energy thresholds of reactions (γ, 2n) and (γ, 3n) correspondingly.

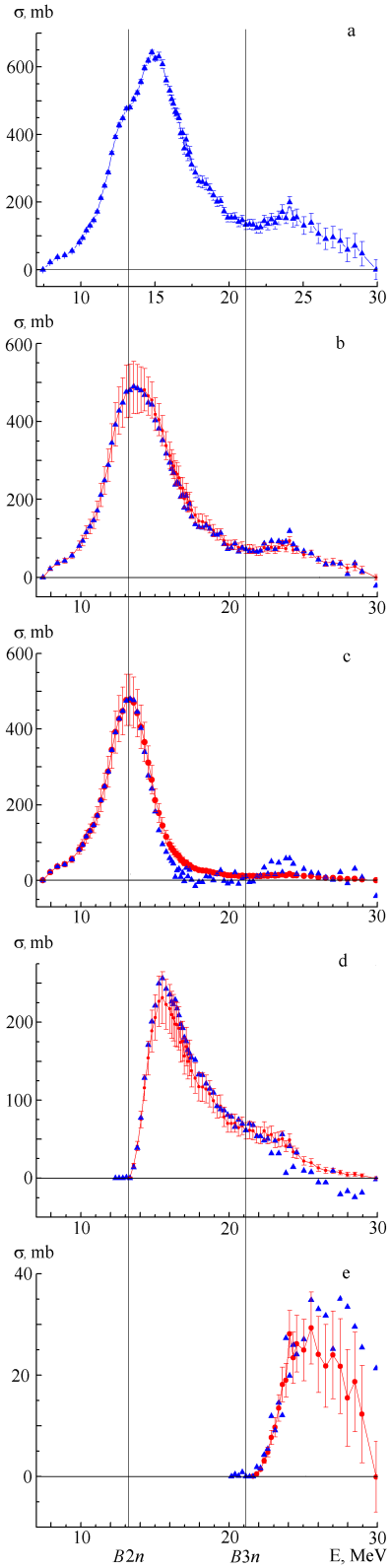

Figure 21. Evaluated (dots) and experimental (triangles, [37]) cross sections of photoneutron reaction cross sections for ^{192}Os: a- $\sigma(\gamma, \mathrm{Sn})$, b- $\sigma(\gamma, \mathrm{tot})$, c- $\sigma(\gamma, 1\mathrm{n})$, d- $\sigma(\gamma, 2\mathrm{n})$, e- $\sigma(\gamma, 3\mathrm{n})$.

Table 7. Comparison of evaluated and experimental [37] integrated till the energy E_{int} cross sections σint (MeV mb) of photoneutron reactions for Os isotopes

Reaction	Experiment	Evaluation
^{186}Os ($E_{\text{int}} = 20.0$ MeV)		
(γ, Sn)	2833.8 (27.8)	2833.8 (27.8)*
(γ, tot)	2345.0 (24.2)	2389.3 (57.5)
(γ, 1n)	1879.2 (23.1)	1967.9 (57.5)
(γ, 2n)	465.8 (7.2)	472.8 (10.3)
^{188}Os ($E_{\text{int}} = 31.0$ MeV)		
(γ, Sn)	4755.0 (58.9)	4755.0 (58.9)*
(γ, tot)	3634.1 (58.5)	3521.4 (74.5)
(γ, 1n)	2633.6 (53.5)	2402.5 (62.8)
(γ, 2n)	880.1 (22.7)	1004.1 (36.6)
(γ, 3n)	120.4 (6.7)	114.7 (16.8)
^{189}Os ($E_{\text{int}} = 31.0$ MeV)		
(γ, Sn)	4715.0 (47.5)	4715.0 (47.5)*
(γ, tot)	3310.3 (54.1)	3341.6 (46.6)
(γ, 1n)	2109.7 (46.6)	2133.0 (39.9)
(γ, 2n)	996.1 (25.9)	1043.4 (20.9)
(γ, 3n)	205.6 (9.3)	165.2 (11.8)
^{190}Os ($E_{\text{int}} = 31.0$ MeV)		
(γ, Sn)	4623.7 (55.1)	4623.7 (55.1)*
(γ, tot)	3251.4 (63.2)	3276.7 (62.5)
(γ, 1n)	2024.9 (51.5)	2068.1 (55.4)
(γ, 2n)	1081.3 (29.3)	1080.6 (25.3)
(γ, 3n)	145.4 (9.7)	138.5 (14.3)
^{192}Os ($E_{\text{int}} = 31.0$ MeV)		
(γ, Sn)	4892.0 (63.4)	4892.0 (63.4)*
(γ, tot)	3305.5 (62.5)	3392.7 (63.4)
(γ, 1n)	1903.1 (54.2)	2032.8 (54.5)
(γ, 2n)	1199.7 (28.4)	1221.8 (28.4)
(γ, 3n)	202.8 (12.2)	138.0 (15.3)

* Experimental [37] neutron yield reaction cross section (22) used as initial for evaluation (26).

9. Photon activation technique

In this section the experimental technique of photon activation analysis is described. Using this technique the photodisintegration of the Os isotopes was studied in the energy ragne of the GDR. For this purpose bremsstrahlung radiation with end-point energy of 67.7 MeV was used. Yields of photonuclear reactions on $^{184,186-190,192}$Os were obtained. Natural osmium was irradiated with bremsstrahlung radiation produced by an electron accelerator with the energy exceeding those of the GDR peak. Different reactions, mainly photonucleon, take place in the target. Stable isotopes of Os, their amount in natural osmium η, and reaction thresholds are shown in table 8. The nuclei produced in the reactions are often β-unstable and after a subsequent decay final nuclei are left in low-lying excited states whose spectra are well-known. Using high-resolution gamma-ray spectrometry this allows one to unambigously distinguish different channels of photodisintegration and to measure yields of the corresponding reactions. An important advantage of this technique is that yields of different reactions on different isotopes can be measured simultaneously and in the same experiment. Effects of dependence of the properties of the GDR on the number of neutrons can be revealed, thus, very accurately.

In the present work the photon activation technique is used to determine the photonucleon reaction yields on stable isotopes of Os. The experimental setup used for this measurement is shown schematically in Fig. 22. The race-track microtron with the maximum electron energy of $E_e = 67.7$ MeV was used [46]. The electron beam struck a tungsten radiator target with the width of 2.1 mm. The bremsstrahlung photons produced in the radiator were directed onto the target made of natural osmium. The target was positioned directly behind the radiator and was large enough to receive almost all produced bremsstrahlung radiation. The irradiation time was about 2 hr. After the irradiation the target was placed on a gamma-ray spectrometer, based on a high-purity germanium detector (HPGe) with 30% relative efficiency. The energy resolution of the detector is 0.9 keV at 122 keV and 1.9 keV at 1.33 MeV. The target was placed as close to the detector endcap as possible. Detection of the residual gamma-ray acitivity of the irradiated target began 6 min after the irradiation and continued for 5 days.

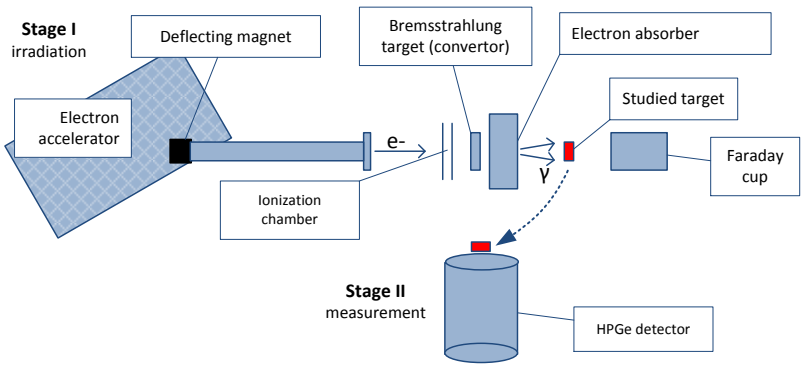

Figure 22. Scheme of the experimental setup used in the photon activation measurements.

The activities of the radioisotopes produced in the osmium target during the irradiations were calculated from the analysis of the gamma-ray spectra using characteristic gamma lines of each radioisotope and their quantum yields η. Prior to this the detection efficiency for different energies of photons was calibrated using reference radioactive sources and a GEANT4 detector simulation program [49]. Figure 23 shows two measured spectra of residual activity at different periods of time after the irradiation. The peaks in the spectra were identified with known gamma-lines of the corresponding nuclei.

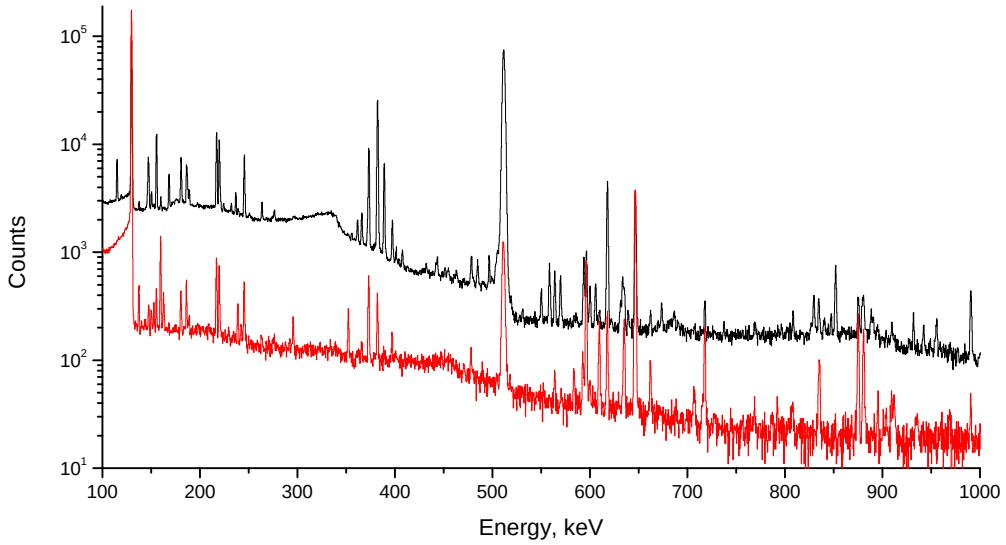

Figure 23. Sample spectra of induced activity: spectrum of a natural Os target 6 min after irradiation (up), duration of measurement 12 h ;5 days after irradiation (down), duration of measurement 12 h. Peaks corresponding to decays with different half-lives can be observed in spectra depending on the time that has passed since the irradiation.

The final result of the photon activation technique are obtained yields of radioactive nuclei produced in photonuclear reactions in the irradiated target. The relationship between the yield $Y(E_m)$ and the cross section $\sigma(E)$ of a photonuclear reaction is through the following expression:

$$Y(E_m) = n \int_{E_{\text{thresh}}}^{E_m} \sigma(E) W(E, E_m) dE, \tag{27}$$

where n is the number of irradiated nuclei in the target, E_{thresh} is the reaction threshold, $W(E, E_m)$ is the spectrum of bremsstrahlung photons with upper energy E_m, that is the number of photons with the energy E per unit interval of energy produced during irradiation with electrons with the kinetic energy $E_e = E_m$.

The photonuclear reaction yields were calculated using the relationship

$$Y(E_m) = \frac{S\lambda}{k(e^{-\lambda(t_2-t_1)} - e^{-\lambda(t_3-t_1)})(1-e^{-\lambda t_1})}, \tag{28}$$

where S is the photopeak area in the residual acitivity spectrum, t_1 is the duration of the irradiation, t_2 is the time of the beginning of the measurement, t_3 is the time of the end of

Table 8. Stable isotopes of Os, their abundances η in natural osmium, reaction thresholds in MeV

Isotope abundance η, %	Reaction threshold B, MeV					
	$(\gamma,1n)$	$(\gamma,1p)$	$(\gamma,1n1p)$	$(\gamma,2n)$	$(\gamma,2p)$	$(\gamma,3n)$
^{184}Os (0.02)	8.66	5.73	14.17	15.79	10.59	24.92
^{186}Os (1.58)	8.26	6.47	14.14	14.89	11.87	23.55
^{187}Os (1.6)	6.29	6.58	12.76	14.55	12.41	21.18
^{188}Os (13.3)	7.99	7.21	14.57	14.28	13.21	22.54
^{189}Os (16.1)	5.92	7.26	13.13	13.91	13.66	20.20
^{190}Os (26.4)	7.79	8.02	15.05	13.71	14.62	21.70
^{192}Os (41.0)	7.56	8.82	15.61	13.32	16.08	21.11

the measurement, λ is the decay constant, k is the coefficient equal to the product of the detection efficiency, true coincidence summing correction factor, and the quantum yield of the given gamma-line.

The calculations properly take into account possible formation of final nuclei not only in nuclear reactions but also as a result of radioactive decay chains. In addition, the effect of isomeric states was taken into account in the same way.

The photon activation technique allows one to measure relative reaction yields. The yields of the produced isotopes were normalized to the yield of ^{191}Os. The ^{191}Os isotope can be produced in the ^{192}Os(γ, 1n)^{191}Os reaction which has a rather high cross section at these energies. In addition, ^{191}Os can be also produced as a result of the ^{192}Os(γ, 1p)^{191}Re reaction with a subsequent β^--decay. The isotopes produced in photonuclear reactions on natural osmium and the yields of the corresponding reactions are shown in table 9.

The experimental yields were compared with calculations using the CMPNR and TALYS models. It is seen that there is a general agreement between the experiment and the calculations. However, it should be mentioned that the proton emission channel is underestimated in the TALYS calculation and is better described by the CMPNR model, where the isospin splitting effect is explicitly included.

10. Synthesis of stable isotopes in nature

The abundance of elements heavier than iron shows little systematic dependence on the mass number A. Production of these elements in charged particle interactions is inhibited by the Coulomb barrier, and, thus, heavy elements are mostly synthesized in neutron capture reactions. There are two kinds of sequential neutron capture processes: the rapid r-process, and the slow s-process. These two mechanisms are different in the value of the ratio of the neutron capture rate to the rate of β-decay. If $\tau_\beta/\tau_n \ll 1$ only stable or long-living nuclei can take part in the nucleosynthesis reaction chain and the process develops along the β-stability valley. This is the s-process, and it apparently ends at lead and bismuth. It is believed that about a half of the observed amount of elements with $A > 60$ are produced in the s-process. The s-process mostly takes place in the shells of red giant stars.

Theoretical estimates show that a neutron density of 10^{10} cm^{-3} is enough for the s-process, and it takes about 10^3 yr to generate lead from the nuclei of the iron peak.

Table 9. Yields of photonuclear reactions on isotopes of Os related to the yield of ^{191}Os obtained in the experiment and calculated using the TALYS and CMPNR models

Isotope	Main reactions	Relative yield		
		TALYS	CMPNR	Experiment
^{191}Os	^{192}Os$(\gamma,1n)^{191}$Os ^{192}Os$(\gamma,1p)^{191}$Re $\xrightarrow{\beta^-}$ ^{191}Os	1.0	1.0	1.0 ± 0.02
^{185}Os	^{186}Os$(\gamma,1n)^{185}$Os ^{187}Os$(\gamma,2n)^{185}$Os ^{188}Os$(\gamma,3n)^{185}$Os	0.0763	0.0741	0.212 ± 0.025
^{183}Os	^{184}Os$(\gamma,1n)^{183}$Os ^{186}Os$(\gamma,3n)^{183}$Os	0.006	0.0037	0.0069 ± 0.0001
^{182}Os	^{184}Os$(\gamma,2n)^{182}$Os ^{186}Os$(\gamma,4n)^{182}$Os	0.0019	0.0009	0.0020 ± 0.0002
^{189}Re	^{190}Os$(\gamma,1p)^{189}$Re	0.0010	0.0063	0.0305 ± 0.0048
^{188}Re	^{189}Os$(\gamma,1p)^{188}$Re ^{190}Os$(\gamma,np)^{188}$Re	0.0013	0.0066	0.0071 ± 0.0022
^{186}Re	^{187}Os$(\gamma,1p)^{186}$Re ^{188}Os$(\gamma,np)^{186}$Re	0.0007	0.0032	0.0041 ± 0.0001
^{184}Re	^{186}Os$(\gamma,1n1p)^{184}$Re	0.0003	0.0020	0.0053 ± 0.0006

If $\tau_\beta/\tau_n \gg 1$, that is if the neutron flux is intense enough (such as during a core-collapsing supernova explosion), then the *r*-process is possible and, in addition to the stable nuclei a large number of β-radioactive nuclei with short lifetimes are included in the nucleosynthesis process. The *r*-process trajectory is shifted from the β-stability valley towards the nuclei with an excess of neutrons. Since a nucleus will keep capturing neutrons until the decay rate doesn't become comparable with the neutron capture rate, the more intense the neutron flux is, the more shorter-living nuclei can be produced in the process. A result of the *r*-process are nuclear abundance peaks at $A = 80, 130, 95$, corresponding to the *s*-process peaks at $A = 90, 138, 208$ and neutron magic numbers $N = 50, 82, 126$. The *r*-process trajectory is blocked as soon as a nucleus with a high α-decay or fission probability appears in the chain.

The cross sections of neutron capture on $^{186-188}$Os were measured in [13] for the energies from 1 keV to 1 MeV. The cross sections from this work are shown in Fig. 25. It should be noted that due to the thermal equilibrium in the stellar medium the atomic nuclei not necessarily capture neutrons while being in the ground state. The probabilities for nuclei to be in an excited state depend on the temperature, and in addition to the (n, γ) process the inelastic neutron scattering (n, n') also becomes more important at higher temperatures. Photodisintegration cross sections on ^{188}Os were measured in [54] using quasimonochromatic laser Compton back-scattered photons. The ^{186,187}Os isotopes together with ^{187}Re constitute an important potential cosmochronometer due to a long half-life of the latter ($41.2 \cdot 10^9$ yr) [53].

While most of the nuclei heavier than iron are synthesized in neutron capture reactions, there is a number of stable neutron-deficient nuclei that do not participate in the *s*- or *r*-process trajectories and whose abundance is 2–3 orders of magnitude less than that of the

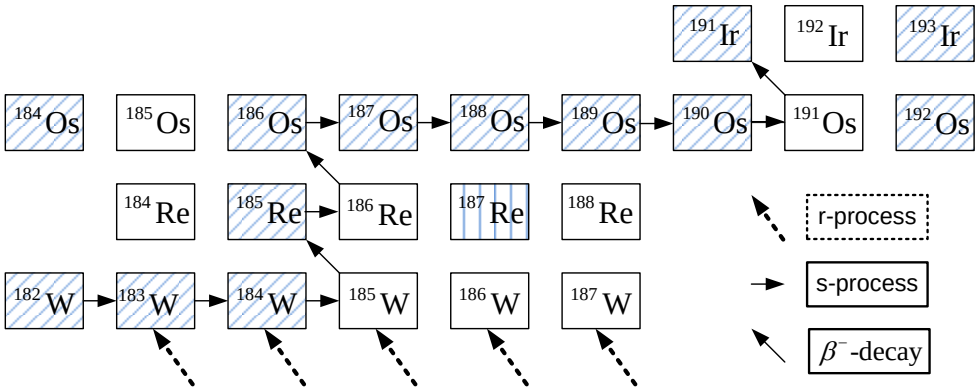

Figure 24. $r-$ and s-processes in W–Ir region. Hatched area denotes stable isotopes.

neigboring nuclei. ^{184}Os is one of such nuclei, called p-nuclei. There are several canditate nuclear reactions to explain synthesis of the p-nuclei:

1. proton capture reactions (p, n), (p, γ);
2. photodisintegration reactions (γ, 1n), (γ, 2n);
3. weak interactions $e^+ + (A,Z) \rightarrow (A,Z+1) + \bar{\nu}_e$;
4. spallation reactions, caused by protons and α-particles generated by a shockwave in the shell of a supernova;
5. neutrino-induced reactions, as in:

$$\nu_e + (A+1,Z-1) \rightarrow (A+1,Z)^* + e^-$$

$$(A+1,Z)^* \rightarrow (A,Z) + n.$$

Another possibility is to consider production of the p-nuclei in photonuclear reactions with several outgoing nucleons. Specifically, the ^{184}Os isotope can be produced as a result of a sequence of (γ, n) reactions starting from stable isotopes of Os in addition to the following multinucleon reactions: ^{186}Os(γ, 2n), ^{187}Os(γ, 3n), ^{188}Os(γ, 4n), ^{189}Os(γ, 5n). Figure 26 shows the cross sections of these reactions calculated using the CMPNR model.

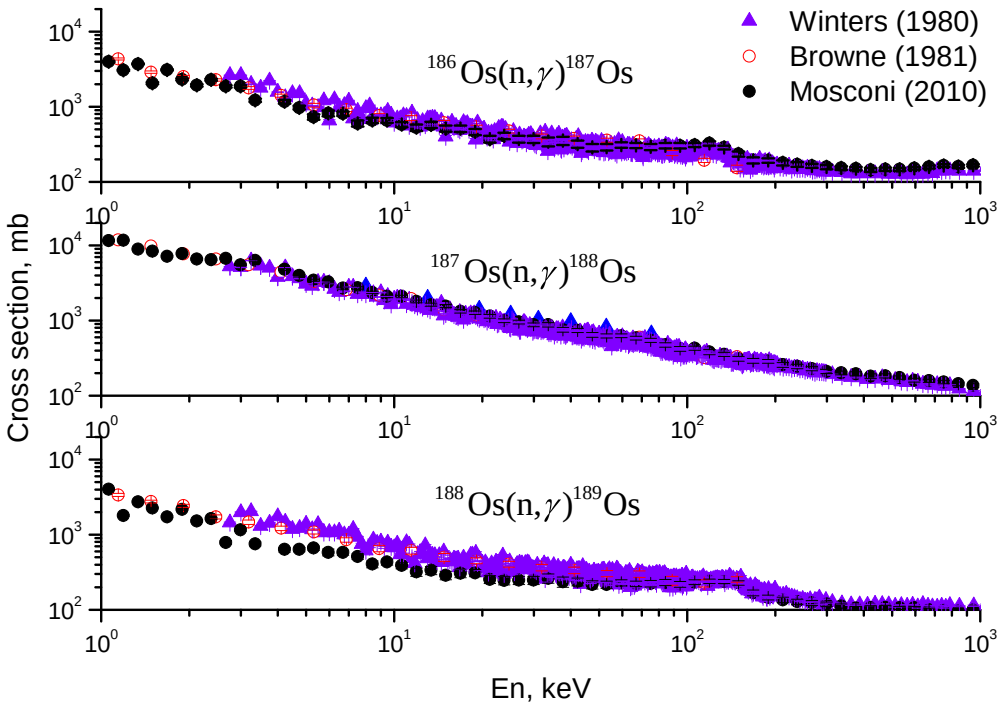

Figure 25. (n,γ) cross section on ^{186,187,188}Os of Winters et al.[51], Browne and Berman [52], and Mosconi et al. [53]

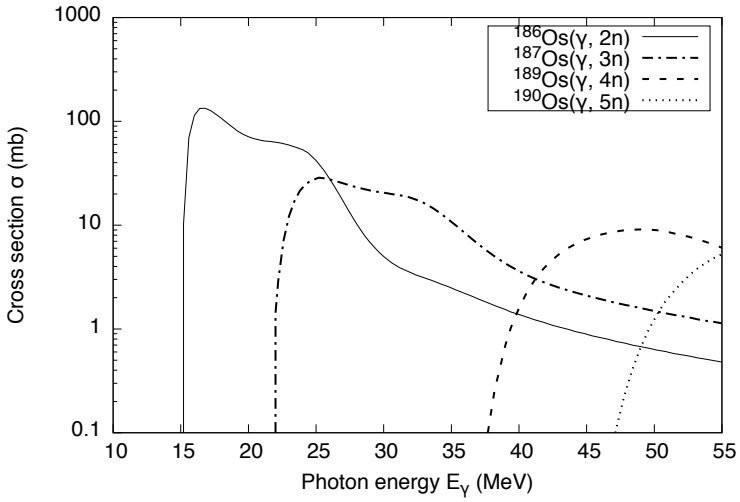

Figure 26. Cross sections of the ^{186}Os(γ, 2n), ^{187}Os(γ, 3n), ^{188}Os(γ, 4n), ^{189}Os(γ, 5n) reactions calculated using the CMPNR model.

11. Conclusions

Some of the practically important nuclear properties of the naturally-present isotopes of osmium, i. e., cross sections and yields of photon-triggered nuclear reactions in the energy range of the giant dipole resonance were considered. Due to the ubiquitous nature of gamma-rays the photonuclear reactions play an important role in most nuclear processes and applications. Available experimental measurements of photonuclear cross sections on the isotopes of osmium were reviewed.

Results of an activation technique-based experiment were reported. The 70-MeV microtron of the SINP MSU was used to generate bremsstrahlung beam and irradiatie the osmium target. After the irradiation the activated nuclear reaction products were identified in the gamma-ray spectra and the yields of the corresponding photonuclear reactions were obtained. The yields of the following reactions were measured: ^{184,186,192}Os (γ, 1n), ^{182}Os(γ, 2n), ^{184}Os(γ, 3n), ^{187,189,190}Os(γ, 1p), ^{186,192}Os(γ, 1n1p), and ^{189}Os(γ, 2p). A first attempt of experimental analysis of reactions with outgoing protons has been made.

Based on the technique from Ref. [35] partial photoneutron reaction cross sections $\sigma(\gamma, 1n)$, $\sigma(\gamma, 2n)$, $\sigma(\gamma, 3n)$ on naturally-present osmium isotopes were evaluated. Reliability criteria were used to estimate the proportion of incorrectly assigned outgoing neutrons in available experimental cross sections.

The obtained results were discussed in connection with the shell structure of the osmium isotopes. As with other heavy nuclei in this region the osmium isotopes reveal a triaxial structure which influences the strength of electromagnetic transitions and thus the probability of photon interactions. Astrophysical aspects of ^{184}Os production in the *p*-process were considered.

References

[1] C. F. von Weizsäcker, Z. Phys. **96**, 431 (1935).

[2] G. Audi *et al.*, Chinese Physics C **36**(12), 1287–1602 (2012).

[3] M. Göppert-Mayer, Phys. Rev. **75**, 1969 (1949).

[4] O. Haxell, J. Jensen, and H. Suess, Phys. Rev. **75**, 1766 (1949).

[5] A. B. Migdal, Zh. Eksp. Teor. Fiz. **15**, 81 (1945).

[6] G. K. Baldwin and G. S. Klaiber, Phys. Rev. **71**, 3 (1947).

[7] S. G. Nilsson, Dan. Mat. Fys. Medd. **29**, 16 (1955)

[8] V. V. Varlamov, "The Map of Parameters of the Shape and Sizes of Nuclei," http://cdfe.sinp.msu.ru/services/radchart/radmain.html.

[9] B. S. Ishkhanov and S. Yu. Troshchiev, Moscow Univ. Phys. Bull. **66**, 325 (2011)

[10] B. S. Ishkhanov and V. N. Orlin, Phys. At. Nucl. **68**, 1352 (2005).

[11] K. Okamoto, Phys. Rev. **110**, 143 (1958).

[12] S. S. Dietrich and B. L. Berman, At. Data Nucl. Data Tables **38**, 199 (1988).

[13] Phys. Rev. C **82**, 015802 (2010).

[14] S. Fallieros and B. Goulard, Nucl. Phys. A **147**, 593 (1970).

[15] K. Kumar and M. Baranger, Nucl. Phys. A **110**, 529 (1968).

[16] R. Sedlmayr, M. Sedlmayr, and W. Greiner, Nucl. Phys. A **232**, 465 (1974).

[17] N. Bohr, Nature 137, 344 (1936).

[18] J. S. Levinger, Phys. Rev. 84, 43 (1951); J. S. Levinger, Phys. Lett. B 82, 181 (1979).

[19] B. S. Ishkhanov, V. N. Orlin, Phys. At. Nucl. **74**, 21 (2011).

[20] B. S. Ishkhanov, V. N. Orlin, Phys. At. Nucl. **76**, 32 (2013).

[21] B. S. Ishkhanov, V. N. Orlin, Phys. At. Nucl. **66**, 688 (2003).

[22] M. B. Chadwick *et al.*, Phys. Rev. C 44, 814 (1991).

[23] B. S. Ishkhanov, V. N. Orlin, Phys. At. Nucl. **78**(6), (2015) [in press].

[24] B.L. Berman, S.S. Fultz, Rev. Mod. Phys. 47 (1975) 713.

[25] S.S. Dietrich, B.L. Berman, At. Data Nucl. Data Tables 38, (1988) 199.

[26] A.V. Varlamov, V.V. Varlamov, D.S. Rudenko, M.E. Stepanov, Atlas of Giant Dipole Resonances (IAEA, Vienna, Austria, 1999) INDC(NDS)-394.

[27] Russia Lomonosov Moscow State University Skobeltsyn Institute of Nuclear Physics Centre for Photonuclear Experiments Data database "Nuclear Reaction Database (EXFOR)", http://cdfe.sinp.msu.ru/exfor; International Atomic Energy Agency Nuclear Data Section "Experimental Nuclear Reaction Data (EXFOR)" database, http://www-nds.iaea.org/exfor; USA National Nuclear Data Center database "CSISRS and EXFOR Nuclear reaction experimental data" database, http://www.nndc.bnl.gov/exfor.

[28] E. Wolynec, A.R.V. Martinez, P. Gouffon et al, J. Phys.Rev. C29 (1984)1137.

[29] E. Wolynec, M.N. Martins, J. Revista Brasileira Fisica 17 (1987)56.

[30] B.L. Berman, R.E. Pywell, S.S. Dietrich et al, J. Phys.Rev. C36 (1987) 1286.

[31] V.V. Varlamov, B.S. Ishkhanov. Study of Consistency Between (γ,xn), [(γ,n) + (γ,np)] and (γ,2n) Reaction Cross Sections Using Data Systematics. Vienna, Austria. INDC(CCP)-433, IAEA NDS, Vienna, Austria, 2002.

[32] V.V. Varlamov, N.N. Peskov, D.S. Rudenko, M.E. Stepanov, INDC(CCP)440, IAEA NDS, Vienna, Austria, 2004, p. 37.

[33] V.V. Varlamov, B.S. Ishkhanov, V.N Orlin, Phys. Atom. Nucl., 75 (2012) 1339.

[34] V.V. Varlamov, B.S. Ishkhanov, V.N. Orlin, N.N. Peskov, M.E. Stepanov. Phys. Atom. Nucl, 76 (2013) 1403

[35] V.V. Varlamov, B.S. Ishkhanov, V.N. Orlin, K.A. Stopani. Eur. Phys. J. A50 (2014) 114.

[36] A.M. Goryachev, G.N. Zalesnyi, S.F. Semenko, B.A. Tulupov. Sov.J.Nucl.Phys. 17 (1974) 236.

[37] B.L. Berman, D.D. Faul, R. A. Alvarez, et al., Phys. Rev. C19 (1979) 1205.

[38] B.S. Ishkhanov, V.N. Orlin. Phys. Part. Nucl., 39 (2007) 232.

[39] B.S. Ishkhanov, V.N Orlin. Phys. Atom. Nucl., 71 (2008) 493.

[40] B.S. Ishkhanov, V.N. Orlin, K.A. Stopani, V.V. Varlamov. Photonuclear Reactions and Astrophysics. In "The Universe Evolution: Astrophysical and Nuclear Aspects", Ed. by I. Strakovsky and L. Blokhintsev. Nova Science Publishers, New York, 2013, p. 113.

[41] V.V. Varlamov, M.A. Makarov, N.N. Peskov, M.E. Stepanov. Bull. Rus. Acad. Sci. Phys., 78 (2014) 412.

[42] V.V. Varlamov, B.S. Ishkhanov, V.N. Orlin, V.A. Chetvertkova, Bull. Russ. Acad. Sci. Phys., 74 (2010) 833.

[43] V.V. Varlamov, B.S. Ishkhanov, V.N. Orlin, S.Yu. Troshchiev, Bull. Russ. Acad. Sci. Phys., 74 (2010) 842.

[44] B.S. Ishkhanov, V.N. Orlin, S.Yu. Troschiev, Phys. Atom. Nucl., 75 (2012) 353.

[45] V.V. Varlamov, V.N. Orlin, N.N. Peskov, M.E. Stepanov, Bull. Russ. Acad. Sci. Phys., 77 (2013) 388.

[46] V. I. Shvedunov, A. N. Ermakov, I. V. Gribov, *et al.*, Nucl. Instrum. Methods A **550**, 39 (2005).

[47] S. S. Belyshev, K. A.. Stopani, Moscow Univ. Phys. Bull. **68**, 88 (2013).

[48] S. S. Belyshev, A. N. Ermakov, B. S. Ishkhanov, *et al.*, Nucl. Instrum. Methods A **745**, 133 (2014).

[49] *Agostinelli S., Allison J., Amako K. et al.* // Nucl. Instr. Meth. Phys. Res. A. 2003. **506**. P. 250.

[50] J. M. Allmond *et al.,* Phys. Rev. C **78**, 014302 (2008).

[51] R. R. Winters, R. L. Macklin, and J. Halperin, Phys. Rev. C **21**, 563 (1980)

[52] J. C. Browne and B. L. Berman, Phys. Rev. C **23**, 1434 (1981).

[53] Mosconi, M., et al., Phys. Rev. C **82**, 015803 (2010).

[54] T. Shizuma, H. Utsunomiya, P. Mohr, T. Hayakawa et al., Phys. Rev. C **72**, 025808 (2005).